ACS OMEGA

http://pubs.acs.org/journal/acsodf

Article

Synthesis, Characterization, and Swelling Properties of a New Highly Absorbent Hydrogel Based on Carboxymethyl Guar Gum Reinforced with Bentonite and Silica Particles for Disposable Hygiene Products

Yahya Bachra,* Ayoub Grouli, Fouad Damiri, X. X. Zhu, Mohammed Talbi, and Mohammed Berrada

Cite This: *ACS Omega* 2022, 7, 39002−39018

Read Online

ACCESS | Metrics & More | Article Recommendations | Supporting Information

ABSTRACT: Superabsorbent polymers derived from petroleum have been widely used as the primary component of high-water-absorption disposable sanitary products. However, environmental concerns as well as unstable market prices influence the quality of disposable hygiene products. The development of superabsorbent polymers from natural, non-petroleum-derived materials has become more predominant. In the present study, two borax-cross-linked carboxymethyl guar-based superabsorbents with bentonite (CMG-Bt) and fumed silica particle reinforcement (CMG-Bt-Si) were synthesized. The materials have been fully characterized by various techniques. The swelling behavior was studied through free swelling capacity (FSC) and centrifuge retention capacity (CRC). The swelling kinetics and urea absorption capacity were further analyzed. The effects of the cross-linking ratio, mineral clay, silica particles, and pH of the liquids on the swelling properties of the superabsorbents have been studied. The incorporation of silica particles demonstrated a positive effect on water uptake reaching 78.63 and 41.09 g/g of FSC and CRC, respectively, at an optimum pH of 6.8. The optimum swelling kinetics were attributed to CMG-Bt-Si of 5 wt % silica particle content, indicating a velocity parameter (ζ) of 41 s in saline solution. Finally, the highest swelling values were obtained at 10, 10, and 5 wt % for the cross-linking ratio, bentonite content, and silica particle content, respectively; in addition, the absorption of urea by the CMG-Bt-Si material was also confirmed.

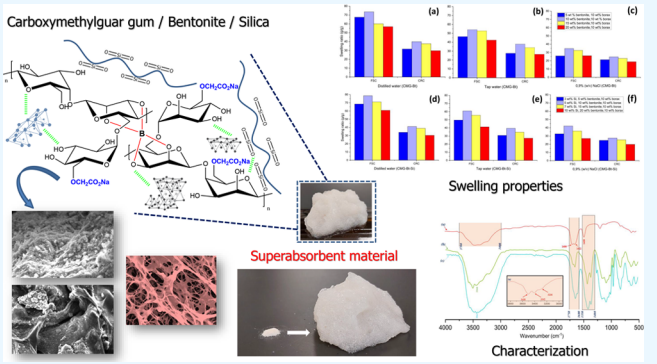

1. INTRODUCTION

Superabsorbent polymers (SAPs) are a class of high-performance synthetic polymers that are distinguished by their outstanding water absorption capacity. These polymers are a type of three-dimensional polymer network, usually composed of ionic monomers, and characterized by a low cross-linking density.[1] A standard SAP is a highly hydrophilic network that has the ability to swell and retain vast amounts of hydrophilic fluids including water, even under pressure. Comparatively, SAPs can absorb up to thousands of times their proper weight in water in a relatively short time, whereas general hydrogels can only absorb about ten times their own mass.[2,3] They have become increasingly important nowadays and are widely used in many fields, including hygiene, biology-related fields, and agriculture.[4,5] Due to their excellent characteristics, SAPs have been applied in many fields, such as disposable hygiene products, including diapers, feminine hygiene products, and adult incontinence articles, which is the largest application area for SAPs, with a market share of over 92%.[6] SAPs are also used in agriculture, forestry, industry, drug delivery systems,[7,8] chemical industry, and water storage to conserve water in dry climates.[9]

Natural gums are green and ecological biopolymers and are considered hydrocolloids. Their byproducts have been employed to synthesize a variety of materials. They are pathological products produced as a result of wounds suffered by a plant and have complex structural characteristics. Their chemical compositions are complex and depend on the type and age of the source as well as the extraction and processing methods.[10−14] Natural gums are obtained from renewable sources in almost every biosphere on the planet, such as microbial, marine, or plant sources.[15] They are categorized as seed gums, microbial gums, or plant exudate gums. Gums are made up of polymers of carbohydrates, including galactose, rhamnose, and uranic acid, moreover and contain functional polar groups such as hydroxyl, carbonyl, and carboxyl groups. The large number of OH groups facilitates the formation of networks with chelating metal ions. Compared to other

Received: July 27, 2022
Accepted: October 10, 2022
Published: October 19, 2022

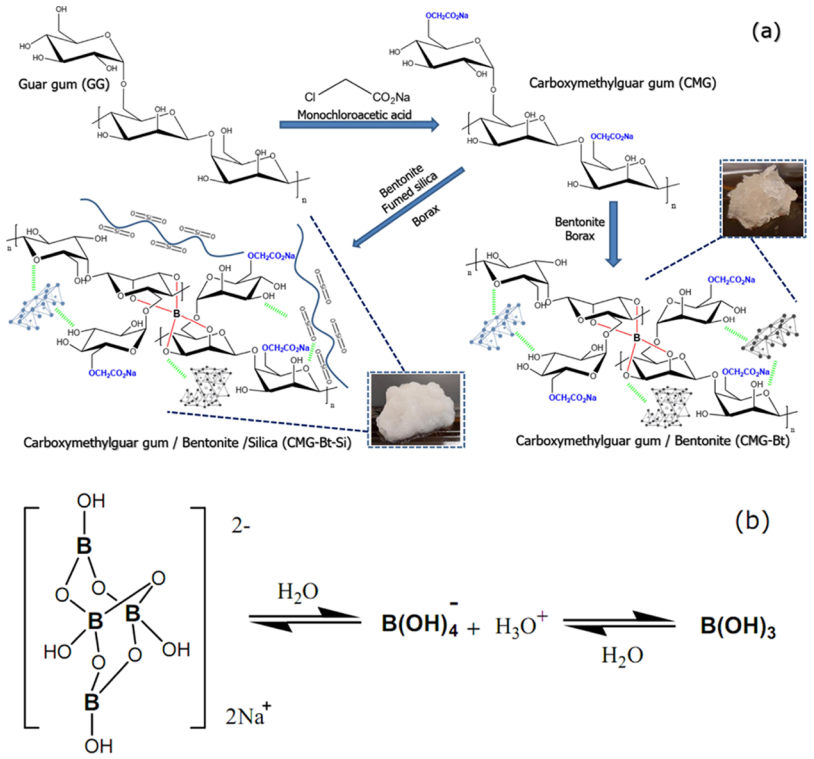

Figure 1. (a) Plausible proposed mechanism for the synthesis of the CMG-Bt and CMG-Bt-Si and the (b) reversible reaction of borax.

biopolymers, gums contain anionic functional groups with a high charge density. The structure of natural gum significantly affects its rheological, thermal, mechanical, optical, and film-forming properties.[16]

Guar gum (GG) was extracted from the seeds of the *Cyamopsis tetragonalobus* plant which is considered a safe and environmentally friendly polymer. It is cultivated commercially in parts of the Asian subcontinent as well as in North Africa and South America, particularly in India, where the climatic conditions are most suitable for growing guar seeds.[10] GG is a biodegradable, nontoxic, abundant, water-soluble, renewable, inexpensive, natural, and environmentally friendly heteropolysaccharide of the galactomannan family. It consists of a linear backbone of β-1,4-linked d-mannose units and is solubilized by the presence of randomly attached α-1,6-linked galactose units as side chains. The ratio of mannose to galactose units varies from 1.5:1 to 2:1, apparently due to climatic variations[17] (Figure 1). Because of its potential to provide a highly viscous solution at relatively low concentrations, its availability, and its cost effectiveness, GG is used extensively in industrial processing applications. The high viscosity of GG solutions is the result of the high molecular weight as well as the presence of numerous intermolecular linkages through hydrogen bonding. Due to its unique properties, GG and its derivatives have found many commercial and industrial uses in water treatment, mining, pharmaceuticals, oilfields, and textiles.[18] Studies have also been conducted using GG and its derivatives as superabsorbent materials for hygienic applications.[19]

The most common SAPs employed in commercial applications have a petrochemical base including poly(acrylic acid) salts and poly(acrylamide) since their monomers are manufactured from nonrenewable petrochemical resources.[20] Superabsorbents of petrochemical origin are usually obtained by free-radical polymerization of vinylic monomers with multifunctional cross-linkers. Synthetic polymers present drawbacks such as nonrecyclability, high market price, energy-consuming synthesis processes, toxicity of trace initiators and unreacted monomers, and environmental concerns.[21,22] In comparison, natural SAPs are prepared from polysaccharides such as chitin,[23] chitosan,[7,24,25] cellulose,[25,26] starch,[27] agarose,[28] alginates,[29] tragacanth,[30,31] tamarind,[32] and carrageenan.[32] They are in great demand in the market due to the continuous increase in the global population and the average age of people. The SAP market is forecast to grow to 12.9 Gb USD by 2024. These statistics are prompting researchers to investigate new superabsorbent materials.[6]

The latest research on new SAPs includes the reswelling mechanism,[33] PVPP-based SAP gel for water retention in sandy soils,[34] carbonaceous SAP/acrylic acid-co-acrylamide,[35] for water and wastewater treatment,[36] biodegradable superabsorbent linseed cake protein-g-poly (acrylic acid)/kaolinite composites,[37] and itaconic acid-based SAPs with improved gel strength.[38] Recently, several guar-based superabsorbents have been developed. These include smart superabsorbent hydrogels,[39] superabsorbent hydrogels for vitamin B6 delivery,[40] and superabsorbents for a controlled micronutrient delivery system,[18] for solid packaging of sugarcane fields, and superabsorbents to improve agriculture under abiotic stress.[41] Similarly, carboxymethylation of guar has been widely used for the structural modification of polysaccharides[42] and for applications such as a sustained transdermal release of some target molecules, sustained release of ciprofloxacin, biomedical applications, agricultural applications, wound healing applications, and tissue engineering applications.[43] Besides, the cross-linking of polymer chains containing cis-diols of polymers with borax has been widely used and recommended.[44−46]

https://doi.org/10.1021/acsomega.2c04744
ACS Omega 2022, 7, 39002−39018

Generally, bentonites are montmorillonite-type mineral clay. They consist primarily of colloidal hydrated aluminum silicate besides containing varying amounts of iron, alkali metals, and alkaline earth metals.[47] Another preferred clay is Laponite, a synthetic smectic clay with a hectorite-like structure. Bentonite is a material composed primarily of montmorillonite (92.2%), K-feldspar (2.7%), plagioclase (1.8%), quartz (1.3%), and calcite (1.0%). Various studies have used bentonite to support the polymeric superabsorbent network.[48] However, the fumed silica (or pyrogenic silica) hydrophilic properties are the combination of hydroxyl groups bound to the silica atoms at the surface of the particle. This allows it to create hydrogen bonds, making it dispersible in water and stable at room temperature.[49] Similarly, the incorporation of silica particles has been widely used in the past for various applications (blended cement, potential hemostatic material, plastic shrinkage cracks, etc.). The incorporation of hydrophilic fumed silica as an additive to create a stable silica−water suspension called "dry water" demonstrates its water retention capacity, subsequently enhancing the retention capacity of the synthesized materials.[50,51] As we know, urea is a metabolite or waste product eliminated by the kidneys. It is a colorless solid and an important source of nitrogen in fertilizers. The normal range of urea is 2.6 to 6.5 mM in human blood and can be 50 times more concentrated with a wide variation in human urine (daily excretion of 342 ± 67 mmol in 490 to 2690 mL of urine). Even though urea is considered safe and nontoxic, at high concentrations and if accumulated on the skin when urine remains in the diaper for a long time, urea can cause rashes, discomfort for the diaper wearers, or psoriasis.[23,52−54] Therefore, superabsorbent materials are expected to absorb urea when they are used in diapers.

Our objective is to develop a new superabsorbent material in the form of an organo-mineral composite that has never been previously made. In addition to its capacity to absorb and retain liquids, this material combines other characteristics, such as excellent absorption kinetics, thermal stability, improved mechanical properties, enhanced absorption, and affinity with urea. Moreover, this synthesis has an environmental approach that promotes the value of products of vegetal and mineral sources, diversifying their uses and taking advantage of their properties for industrial purposes such as GG and bentonites. All these characteristics render the superabsorbent product competitive with commercial products in terms of the quality−price ratio. In this study, two superabsorbent materials were synthesized. A carboxymethyl guar-based material reinforced with bentonite later called CMG-Bt and, also, a second material based on carboxymethyl guar reinforced with bentonite and incorporated with fumed silica particles later called CMG-Bt-Si.

2. MATERIALS AND METHODS

2.1. Materials. GG (research-grade, M_w = 200 kDa) was obtained from Sigma-Aldrich and then used with no additional purification. Gray bentonite (Bt) (supplied by Sigma-Aldrich) was used without further purification. Fumed silica (Si) (SiO_2, powder, average particle size of 0.2−0.3 μm) was also purchased from Sigma-Aldrich. Boric acid (grade II) was used to prepare the cross-linker, which was purchased from Loba Chemie (India). Monochloroacetic acid, glacial acetic acid, hydrochloric acid, anhydrous sodium carbonate, sodium chloride, and sodium hydroxide were of analytical grade (extra-pure) and were used, with no additional purification, as supplied by Sigma-Aldrich (USA). Methanol and ethanol were of standard analytical grade (99.7% purity) and were obtained from VWR Chemicals (USA). Saline solution was used as 0.9% (w/v) NaCl for use in the study of SAP swelling behavior, and sodium chloride was of analytical grade (99% purity) from Loba Chemie (India). The hardness of the tap water was between 100 and 140 ppm calcium carbonate. The acidic and basic solutions used, to adjust the pH, were prepared by diluting hydrochloric acid (pH 1.0) and sodium hydroxide (pH 13.0) solutions with distilled water.

2.2. Experimental Section. Superabsorbent materials were synthesized using three steps. First, carboxymethyl guar (CMG) was synthesized via the carboxymethylation process, then the material was reinforced with bentonite fractions and silica particles, and in the last step, the cross-linked materials were produced by cross-linking using borax as the cross-linker. Structural characterization of the superabsorbent materials was performed by 1H nuclear magnetic resonance (NMR), 13C NMR, degree of substitution (DS), Fourier transform infrared spectroscopy (FTIR), thermogravimetric analysis (TGA), differential thermal analysis (DTA), differential scanning calorimetry (DSC), X-ray diffraction (XRD), scanning electron microscope−energy-dispersive X-ray spectroscopy (SEM-EDAX), and elemental analysis. Swelling performance was studied by FSC and CRC. Swelling kinetics and urea absorption capacity were also analyzed. Analysis of the swelling properties of the SAP was investigated by studying the effect of cross-linking ratios, mineral clay, and silica particles on water absorption. In addition, the effect of the nature and pH of the liquids on the performance of the superabsorbent materials was also determined.

2.2.1. Synthesis of CMG. In a round-bottom flask equipped with a mechanical stirrer, 2 g of GG was dispersed in 100 mL of deionized water and kept under stirring overnight, and then, the solution was sonicated for 1/2 h to remove air bubbles until a clear colloidal solution was obtained. Then, 10 mL of NaOH (10%) was added to the previous solution slowly (1 mL/min) and stirred for 15 min at room temperature. Next, 5 g of monochloroacetic acid was dissolved in 15 mL of deionized water and added to the previous solution over 10 min at a rate of 0.5 g/min. After 30 min of constant stirring, the reaction mixture was heated to 60 °C for 4 h. The reaction mixture was extracted with excess ethanol and then centrifuged 3 times. The pH of the extracted mixture was adjusted to 7 using glacial acetic acid. Then, 50 mL of cold ethanol was added to the reaction mixture as a nonsolvent and the precipitate was collected, washed several times with excess methanol, and dried under a vacuum. Finally, the resultant product was milled and sieved. The yield of the synthesis was about 72%. The CMG obtained is kept in a dry condition for subsequent use.

2.2.2. Cross-Linker Preparation. Borax was selected to be used as a cross-linker in the synthesis of the following superabsorbent materials. The preparation of borax from boric acid was chosen and prepared by the classical and efficient method. In a 200 mL beaker, 25 g of boric acid was added to 80 mL of deionized water, and then, the boric acid was dissolved with heating and gentle stirring. The mixture was added to a previously prepared solution of 11.2 g of dissolved anhydrous sodium carbonate, the mixture was then boiled, and heating was stopped when effervescence was complete. Finally, colorless crystals of borax were recovered after cooling the solution and then kept dry for later use.

https://doi.org/10.1021/acsomega.2c04744
ACS Omega 2022, 7, 39002−39018

2.2.3. Synthesis of CMG-Bt & CMG-Bt-Si. The synthesis is elaborated in an orthogonal model as described in Table 1,

Table 1. Synthesis Conditions of CMG-Bt & CMG-Bt-Si: Reagent Proportions (wt %) and Swelling Performances in Distilled Water (g/g)

		reagent proportions (wt %)			swelling performances (g/g)	
N°	sample	borax	bentonite	fumed silica	FSC	CRC
1	CMG-Bt 01	5	0		34.98	25.87
2	CMG-Bt 02	5	5		37.69	31.59
3	CMG-Bt 03	5	10		38.65	35.45
4	CMG-Bt 04	5	15		35.24	32.2
5	CMG-Bt 05	5	20		33.58	30.29
6	CMG-Bt 06	10	0		46.25	29.33
7	CMG-Bt 07	10	5		67.5	31.58
8	CMG-Bt-Si 01	10	5	3	68.52	33.97
9	CMG-Bt 08	10	10		73.58	39.91
10	CMG-Bt-Si 02	10	10	5	78.63	41.09
11	CMG-Bt 09	10	15		60.11	37.58
12	CMG-Bt-Si 03	10	15	7	71.09	38.89
13	CMG-Bt 10	10	20		56.83	29.66
14	CMG-Bt-Si 04	10	20	10	60.8	30.29
15	CMG-Bt 11	15	0		44.08	28.13
16	CMG-Bt 12	15	5		48.31	34.86
17	CMG-Bt 13	15	10		48.47	33.97
18	CMG-Bt 14	15	15		42.35	37.12
19	CMG-Bt 15	15	20		42.85	36.27
20	CMG-Bt 16	20	0		24.35	18.5
21	CMG-Bt 17	20	5		21.98	17.4
22	CMG-Bt 18	20	10		20.45	20.66
23	CMG-Bt 19	20	15		21.96	17.26
24	CMG-Bt 20	20	20		18.23	14.23

wherein borax, bentonite, and fumed silica were used in different proportions of the weight of GG. CMG was suspended in 150 mL of deionized water and stirred with a magnetic stirrer. Then, 3 mL of sodium hydroxide solution (30%) was added and the mixture was heated to 60 °C for 2 h. In the meantime, a bentonite solution was prepared by hydrating a quantity of pure bentonite in 10 mL of distilled water at 50 °C. The bentonite suspension was added to the CMG dispersion and left to react for 1 h. Then, an amount (wt %) of fumed silica was incorporated into the reaction mixture and stirred for 2 h. Solutions of different concentrations of borax were gradually deposited under stirring without heating until the so-shaped gel was fully formed. Then, the formed gel was mixed with excess methanol around 200 mL, triturated, and transferred to a beaker. The pH was adjusted to 7.91 under vigorous mechanical stirring using hydrochloric acid (10%). The resulting solid was filtered, washed with methanol, and dried overnight at 60 °C until the product weight remained constant. The products, subsequently named CMG-Bt and CMG-Bt-Si, were finely ground to obtain a superabsorbent material reinforced with a mineral charge.

2.3. Characterization. *2.3.1. Nuclear Magnetic Resonance Spectroscopy (^{1}H NMR/^{13}C NMR).* ^{1}H NMR spectra of GG and CMG were recorded on a 500 MHz NMR spectrometer (Ultrashield plus, Bruker Inc., Billerica, MA, USA) equipped with Bruker's 3.2 mm DVT probe. Dry samples of GG and CMG were dissolved in D_2O-NaOD at a probe temperature of 70 °C.[55] The ^{13}C NMR spectra of pure GG (c) and CMG (d) were collected by solid-state NMR technique, which were recorded on a 600 MHz NMR spectrometer (Ultrashield, Bruker Inc., Billerica, MA, USA) at 30 °C. Data analysis was achieved with MestReNova software, version 11.0.4.

2.3.2. Fourier Transform Infrared Spectroscopy (FTIR). FTIR spectra of GG, CMG, CMTG-Bt, CMTG-Bt-Si, and urea were recorded with KBr pellets prepared on a Bruker Tensor-27 spectrophotometer from Bruker Corporation, Germany. The infrared transmittance method was performed, and all spectra were an average of 32 scans from 4000 to 400 cm^{-1} at a resolution of 4 cm^{-1}. However, the spectra of bentonite, borax, and fumed silica were an average of 32 scans from 2000 to 400 cm^{-1} at the same resolution.

2.3.3. Thermogravimetric and Thermodifferential Analysis (TGA-TDA). TGA and DTA of GG, CMG, CMG-Bt, and CMG-Bt-Si were carried out using a Setsys Evolution 16/18 TGA/DTA instrument (SETARAM). Samples were subjected to a heating rate of 10 °C/min in a heating range of 42−600 °C.

2.3.4. Differential Scanning Calorimetry (DSC). The thermal stability of the prepared CMG-Bt-St samples was obtained using the DSC technique (SDT Q600 V20.9 Build 20 instrument). A platinum tray was used to heat the sample at 10 °C/min from 20 to 600 °C under an N_2 atmosphere (100 mL/min).

2.3.5. X-ray Diffraction Analysis (XRD). XRD patterns of GG, CMG, CMTG-Bt, and CMG-Bt-Si were analyzed using a Bruker D8-Advance powder diffractometer (Germany) equipped with nickel-filtered Cu-Kα radiation (λ = 1.54056° A) at a specific voltage and current (40 kV,100 mA). The scattered radiation was detected in the angular range of 10−60° (2θ), with a step-counting method (step 0.01° 2θ) in continuous mode.

2.3.6. Scanning Electron Microscope/Energy-Dispersive X-ray Spectroscopy (SEM−EDX). Morphological analysis of the samples was performed with a scanning electron microscope (SEM−EDX) using a Hirox MiniSEM Model SH-4000 M with an accelerating voltage of 20 kV at different magnifications. The samples were freeze-dried prior to the scanning.

2.3.7. Elemental Analysis. The elemental analysis of CMG-Bt-Si in a pure state and another state after absorbing urea was performed, at Université de Montréal (Département de Sciences biologiques, Complexe des Sciences MIL), with a Carlo Erba 1108 elemental analyzer. The estimation of only carbon and nitrogen was estimated.

2.4. Swelling Properties. Analogously, FSC and CRC methods are industrial grades for absorption tests. As they are recognized by international organizations and recommended by absorption assessment standards for SAPs to be applied to assess the synthesized materials.[56] It is noted that the tests were carried out at a temperature of 23 ± 2 °C with a relative humidity of 50% and that the samples were conditioned for 8 h before testing.

2.4.1. Free Swell Capacity (FSC). FSC refers to the amount (g) of liquid absorbed per gram of composition. It is known as the teabag method. This method is the most convenient and fastest way to assess the absorbency of the absorbent sample. The tester fluids are distilled (demineralized) water, tap water (100−140 ppm $CaCO_3$), and a saline solution (0.9 wt % NaCl solution). Teabags were filled with (0.5 g ± 0.01) CMG-Bt and CMG-Bt-Si samples with different proportions of

https://doi.org/10.1021/acsomega.2c04744
ACS Omega 2022, 7, 39002−39018

bentonite and silica particles, uniformly distributed in the teabag, immersed in tester liquid for 30 min, lifted out to reach equilibrium swelling, let to stand for 10 min to release excess solution, and then weighed. Empty teabags were also prepared and run through the same steps to serve as controls. Controls were prepared for each test sample to determine the average absorption factor (F, g/g) of the empty teabag according to eq 1.

$$F\ (\mathrm{g/g}) = (T_2 - T_1)/T_1 \tag{1}$$

where F, T_2, and T_1 are the absorption factor of the teabag, the weight of the empty stretched teabag (control), and the weight of the empty dry teabag (control), respectively. Therefore, the FSC was calculated using the following equation (eq 2).−

$$\mathrm{FSC}\ (^{\mathrm{g}}/_{\mathrm{g}}) = (W_2 - (W_1 - \overline{F}) - W_1 - W_0)/W_0 \tag{2}$$

where W_2 is the weight of the inflated sample, W_1 is the weight of the empty dry tea bag, W_0 is the initial weight of the superabsorbent material sample, and $\overline{F}$, mathematically, is the average absorption factor of the teabag (g/g). The free absorption of each particulate sample was determined by averaging the results of three tested samples.

2.4.2. Centrifuge Retention Capacity (CRC). The CRC approach refers to the ability of CMG-Bt and CMG-Bt-Si samples to retain fluid after being saturated and centrifuged under controlled conditions. The resulting retention capacity was measured in grams of fluid retained per gram of sample weight (g/g). The test samples were the same teabags (including controls) recovered from the previous FSC test. The teabags were placed in a suitable centrifuge equipped with a basket rotor capable of subjecting the samples to a g-force of approximately 250 G applied to a mass placed on the internal wall of the basket.

The teabags were placed on the basket, centrifuged at 1400 rpm for 5 min, removed, and weighed. The volume of solution retained by the sample, including the solution retained by the teabag itself, was the CRC of the samples. However, the retention factor (F, g/g) of the teabag controls (blanks) was also calculated using eq 1. The retention was then calculated using the following equation (eq 3):

$$\mathrm{CRC}\ (^{\mathrm{g}}/_{\mathrm{g}}) = (W_2 - (W_1 - \overline{F}) - W_1 - W_0)/W_0 \tag{3}$$

where W_2 is the weight of the centrifuged teabag (g), W_1 is the weight of the empty, dry teabag (g), W_0 is the initial weight of the superabsorbent material sample (g), and $\overline{F}$ is the average retention factor of the teabag (g/g). Three trials of each particle sample were tested, and the results were averaged to determine the CRC values.

2.4.3. Absorption Rate (AR). The purpose of this method is to determine the rate of absorption capacity over the immersion time (AR) of CMG-Bt and CMG-Bt-Si samples in saline solution at various time intervals. The sample was weighed and then filled into teabags, which were placed in saline solution and left free of absorption at different immersion time intervals. Based on the immersion times, the teabags were removed and hung up to let the excess liquid fall out. Finally, the teabags were weighed to determine the amount of liquid absorbed. The teabags (including blanks) were prepared and filled with the SAP sample as described in the FSC protocol. Then, the teabags were immersed in saline solution for 30, 60, 180, 300, 900, and 1800 s, removed to reach equilibrium swelling, left for 15 min to drain off excess solution, and then weighed. Thus, the absorption rate (AR, g/g) was calculated using eqs 2 and 3 above.

2.4.4. Absorption of Urea. A urea solution is prepared at the equivalent concentration of urine urea for a 1−2 years old (20 mg/dL). Then, 0.5 g of CMG-Bt and CMG-Bt-Si samples were put in teabags and immersed in the prepared urea solution for 30 min, dried for 1 h at room temperature, and then dried under vacuum in order to remove the maximum amount of absorbed water. Finally, the samples were analyzed by FTIR, DSC, and elemental analysis by the methods described above to confirm the urea uptake.

3. RESULTS & DISCUSSION

3.1. Synthesis of Superabsorbent Materials. As is known, the swelling ability in water can be enhanced by increasing the hydrophilic moieties and hydrogen bonds in the polymer backbone. GG has a hydrophilic behavior and can disperse in the presence of an aqueous medium, due to the availability of hydroxyl groups −OH on the β-D-mannose chains and the α-D-galactose ramifications. According to this hypothesis, this synthesis aimed to provide swelling capacity in GG to convert it into a superabsorbent material. The process involved increasing the number of anionic groups on the galactomannan chains and then partially cross-linking these chains by organic synthesis instead of radical random polymerization using acrylic or acrylamide monomers. The grafting of anionic groups into GG chains involves a chemical reaction commonly reported as the Williamson etherification reaction. This is an etherification process between alkaline galactomannan and sodium chloroacetate or what is known as the carboxymethylation process. Indeed, it is considered a nucleophilic substitution reaction. Nucleophilic substitution is a reaction in which there is a selective attack by an electron-rich nucleophile on the electrophilic site (i.e., on an electrophilic carbon atom) that links with a leaving group by a covalent bond so that the nucleophile subtract will replace the leaving group.

In this case, CMG, a two-step consecutive reaction, proceeding with a strong base, such as sodium hydroxide, deprotonates the free hydroxyl groups ($-CH_2OH$) in GG to form carboxylate moieties, thus increasing their nucleophilicity as well as the negative charge density. Carboxymethyl groups ($-CH_2-COOH$) are then formed in a reaction between monochloroacetic acid and guar alkoxides. A secondary reaction takes place simultaneously, resulting in the formation of sodium glycolate from sodium chloroacetate and sodium hydroxide. Carboxymethylation generally depends on four main factors that influence the efficiency of the carboxymethylation process: the volume and concentration of sodium hydroxide, the weight of monochloroacetic acid, and the reaction temperature. Based on the previous studies reported, the optimal ratios were selected for this study.[45,56] The resulting CMG is a modified polymer with a variety of reactive carboxylate groups that convert it into a hydrophilic material capable of attracting water and polar molecules. Furthermore, it is also capable of forming new bonds by reacting with reactive groups. Indeed, it should be noted that the carboxymethylation must be limited in order to maintain free hydroxyl groups for cross-linking and hydrogen bonds to stabilize the mineral clays added afterward. However, it must be partially cross-linked to pass to the superabsorbent grade.

As reported, bentonite clay is a water-swellable but water-insoluble organic polymeric hydrocolloid, allowing for

https://doi.org/10.1021/acsomega.2c04744
ACS Omega 2022, 7, 39002−39018

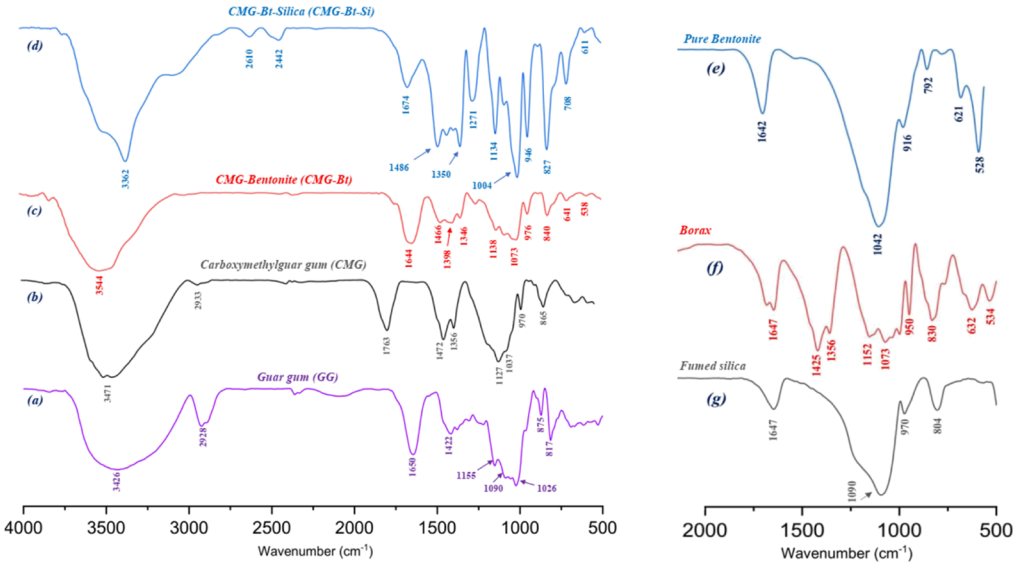

Figure 2. FTIR spectra: (a) GG, (b) CMG, (c) CMG-Bt, (d) CMG-Bt-Si, (e) pure bentonite, (f) borax, and (g) fumed silica.

enhanced absorption for swelling applications. Superabsorbent hydrogels prepared by mixing CMG-dried hydrogels with bentonite clay powder before cross-linking can be effective in enhancing and sustaining the swelling performance of the material, via the physical bonding between Si−OH and O−H of bentonite and CMG functional groups. As the silica nanoparticle (SiO_2), dioxosilane (O═Si═O) is the coordination of silicon (46.83%) and oxygen (53.33%). In addition to being a filler, it has been shown that coating with silicon dioxide in commercial epoxy resin has great importance in improving hydrogel performance, and incorporating silica nanoparticles was an exceptional technique for making polymer nanocomposites. Moreover, these are in the form of silanol groups and show strong reactivity toward the hydroxyl group of CMG, which contributes the most to the development of strength in superabsorbent products.[38]

Borax is the cross-linker chosen to prepare the tree hydrogel. Sodium tetraborate is a well-documented boron derivative for cross-linking cis-diols, in particular for cross-linking GG and its derivatives. CMG is prepared by cross-linking GG with borax (disodium tetraborate and decahydrate) in, via borate ions, basic aqueous solutions at room temperature. Borax dissolves in water and readily decomposes into borate ions and boric acid, forming an alkaline borate/borate solution. The cross-linking process is divided into two steps, monoidal complexation followed by a cross-linking reaction to form the diol−borax complex. Finally, the superabsorbent materials with a three-dimensional network were obtained. The formation of carbon−oxygen−borax−oxygen bonds between the CMG and the boron center during cross-linking is unstable at a certain energy value while leading to a semi-interpenetrating hydrogel formation. The environment-friendly natural guar base, without the use of added artificial monomers or toxic cross-linkers in the formation process of superabsorbent materials, facilitates the biodegradation mechanisms of the superabsorbent after use, which is an advantage over commercial SAPs on the market.

3.2. Structural Characterization. *3.2.1. Nuclear Magnetic Resonance Analysis.* The ^{1}H NMR spectra of pure GG (a) and CMG (b) as well as ^{13}C NMR spectra of pure GG (c) and CMG (d) are illustrated in Figure S1. Further, the nuclear magnetic resonance analyses were performed to confirm the synthesis of CMG, as solid-state NMR spectroscopy is an atomic-level approach usually applied to confirm the chemical structure of the samples.

In the ^{1}H NMR spectrum of GG, the peak corresponding to D_2O-d was removed to overcome overlaps with the other peaks to adequately interpret the rest of the peaks in the same region, due to the dominance of the solvent peak. Generally, in the ^{1}H NMR spectra of GG and CMG, the anomeric protons were localized as signals at 4.6−5.4 ppm, while the non-anomeric protons were localized at 3.2−4.2 ppm. The anomeric protons of GG were observed at δ (5.02 and 4.75 ppm) which are attributed to β-mannopyranosyl and α-galactopyranosyl units, respectively, while the peaks located at δ (3.66−4.11 ppm) are attributed to the cyclic sugar protons.[57] However, in the ^{13}C NMR spectrum of GG, the anomeric carbons were observed at 102.64 ppm, while the remaining carbons in the ring were observed between δ (40−80 ppm). The peak at δ (74.53 ppm) was related to the carbon atoms connected by −OH groups such as in the six-membered ring, except for the anomeric carbon atom in the case of α-D-galactose and β-D-mannose units, and another peak at δ (63.5 ppm) was attributed to the carbon at the C_6 position ($-CH_2OH$ group).[58]

As is seen in the ^{1}H NMR spectrum of CMG, the anomeric protons of CMG were observed at δ (4.96 and 4.68 ppm), whereas the spectrum for CMG revealed the appearance of new proton peaks at δ (3.74, 3.89, and 4.2 ppm), ascribed to methylene protons in the carboxymethyl substituents at the C_6 position of the α-D-galactose unit and the C_3−C_6 positions of the β-D-mannose unit. However, in the ^{13}C NMR spectrum of CMG, similarly to the peaks present in GG spectra, the anomeric carbons were observed at δ (100.75 ppm), while the remaining carbons in the ring were observed between δ (50.32 and 71.65 ppm). In the case of CMG, there were supplementary peaks. A signal at δ (81.66 ppm) in overload with the peak at δ (71.65 ppm) mentioned earlier was attributed to the carbon at the α-position to the carbonyl group of the carboxymethyl group ($-O-CH_2$-). In addition, at 181.29 ppm, a peak was attributed to the carboxyl carbon atom (C═O) of $-COO^-$ Na^+.[43,57] Therefore, the presence of

https://doi.org/10.1021/acsomega.2c04744
ACS Omega 2022, 7, 39002−39018

additional peaks in the CMG spectra was providing a significant support for the grafting of the carboxymethyl group on the GG chain matrix, consequently, confirming the CMG synthesis.

3.2.2. Determination of the Degree of Substitution (DS). ^{1}H NMR analysis was performed also to investigate the DS of CMG. The DS is defined as the average number of substituted groups attached per unit of anhydroglucose, whose value is 3 for GG. Theoretically, the DSs can therefore range from 0 to 3 (completely substituted). However, as known, primary hydroxyl groups are much more reactive than secondary hydroxyl groups. If only the primary hydroxyl groups react, the maximum DS is 0.67.[59] The partial DS (carboxymethylation) was determined from the ^{1}H NMR spectra, using the integral (area) of the proton peaks between chemical shifts of 3.5−5.2 ppm, according to eqs 4, 5, and 6.[43,60]

$$DS_{man} = \frac{A_{(\text{CMG protons@C6 of mannose})}}{A_{(\text{CMG protons@C6 of mannose})} + A_{(\text{GG protons@C6 of mannose})}} \quad (4)$$

$$DS_{man} = \frac{A_{(\text{CMG protons@C6 of galactose})}}{A_{(\text{CMG protons@C6 of galactose})} + A_{(\text{GG protons@C6 of galactose})}} \quad (5)$$

$$DS = DS_{man} + DS_{gal} \quad (6)$$

where DS_{man} represents the DS on the β-D-mannose unit, DS_{gal} represents the degree of substitution on the α-D-galactose unit, A represents the area of the proton peak, and DS is the partial DS representing the degree of carboxymethylation of the C_6 hydroxyl groups of the α-D-galactose unit and the β-D-mannose unit in the polymer chains of GG. Based on the NMR data of the spectra in Figure S1, the DS was determined to be 0.19.

The DS value obtained is considered as a carboxymethylation rate of 28.35% (concerning the DS of the complete substitution), i.e., the grafting of the carboxymethyl group onto the guar backbone. However, the DS (0.19) is considered appropriate because the grafting rate of anionic groups onto the polymer chain required to produce a superabsorbent material is in the range of (25−30%).[61−63]

3.2.3. FTIR Analysis. The FTIR spectra of neat GG (a), CMG (b), CMG-Bt (c), and CMG-Bt-Si (d) are shown in Figure 2. Generally, the characteristic bands of the galactomannan backbone are observable in all spectra. The most important bands for identification and characterization are discussed further below. Figure 2a shows the characteristic bands of GG. The broadband in the wavenumber range between 3090 and 3600 cm^{-1} centered around 3426 cm^{-1} is attributed to the O−H stretching vibration with intermolecular hydrogen bonding, followed by C−H symmetrical stretching vibrations of the group CH_2 at 2928 cm^{-1}. The absorption band at 1650 cm^{-1} is due to ring stretching, while the significant absorption peaks at 1155, 1090, and 1026 cm^{-1} show the C−OH bond, CH_2OH stretching, and CH_2 twitch vibrations, respectively. Typical bands at 875 and 817 cm^{-1} for galactose and mannose are similarly identified. Characteristic bands at 875 and 817 cm^{-1} are related to galactose 1−4 and mannose 1−6 linkages, respectively, and are also recognized.

The CMG FTIR spectrum is shown in Figure 2b, and the bands centered at 3471, 2933, 1137, 971, and 865 cm^{-1} are assigned to the same vibrations of GG as previously discussed. A strong band at 1763 cm^{-1} is attributed to the stretching vibration of the C═O single bond of the ester carbonyl group in addition to two successive stretching vibrations of the methyl group appearing at 1472 and 1356 cm^{-1}. The band that appears at 971 cm^{-1} results from the C−O−C stretching of the CMG glycoside bond.[64,65] Indeed, the appearance of the bands proves the current modification of the glycosidic backbone of the GG.

Then, Figure 2c,e,f represent the FTIR spectra of CMG-Bt, pure bentonite, and borax, respectively. In addition to the bands characterizing the CMG as discussed above, other unique bands appear that approve the formation of the borax cross-linked polymer. The broad peak observed in Figure 2c at 3544 cm^{-1} was slightly reduced to a marginally thin and sharp band with a slight shift to an extended wavelength. This has been attributed to the involvement of hydroxyl groups from the galactomannan chains in the formation of covalent bonds with the cross-linker, and thus, the dynamic borate/diol bonds between the OH groups distributed on the CMG backbone and $B(OH)^{4-}$ could be created.

By comparing the spectra in Figure 2d,g, it can be seen that the Si−OH and C−OH absorption bands (3400−3200 cm^{-1}) were found to be more intense for CMG-Bt-Si. Some band vibrations for fumed silica (1080−850 cm^{-1}) are very intense compared to previous spectra. The newly formed bond of Si−O−Si in the spectrum of fumed silica (Figure 2g) was observable at 1134 cm^{-1}, which confirms the existence of silica nanoparticles. Additional stretching vibrations were observed at 1674, 1007, and 970 cm^{-1} for the C−C and Si−O−C fragments present in the SAP. Similarly, several bands ranging between 950 and 500 cm^{-1} related to pure bentonite, borax, and fumed silica, observed in Figure 2e,f,g respectively, are also visible in the CMG-Bt and CMG-Bt-Si spectra demonstrating that the cross-linking of the polymer by borax additionally confirms the existence of pure bentonite nanoparticles and fumed silica nanoparticles between the polysaccharide chains reinforcing the three-dimensional network.

3.2.4. Thermal Analysis. Figures 3 and 4 represent the thermogravimetric and thermodifferential curves of GG (a),

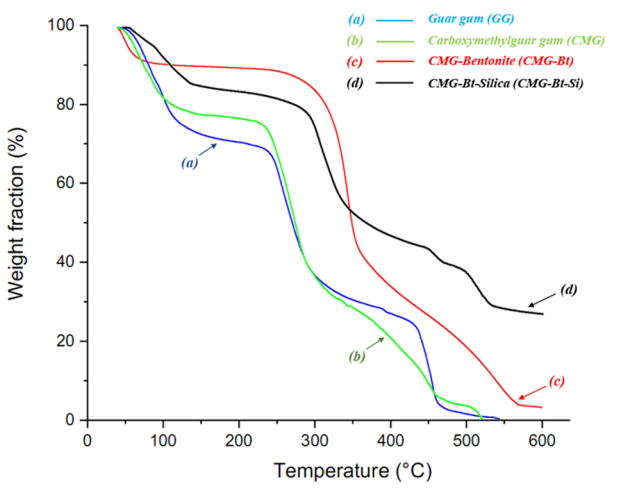

Figure 3. TGA curves of (a) GG, (b) CMG, (c) CMG-Bt, and (d) CMG-Bt-Si.

CMG (b), CMG-Bt (c), and CMG-Bt-Si (d), respectively. As is widely reported, the decomposition of polysaccharides comprises four major steps and there are some cases of combined loss steps: first, desorption of physically absorbed water; excretion of bound water by dehydration reactions;

https://doi.org/10.1021/acsomega.2c04744
ACS Omega 2022, 7, 39002−39018

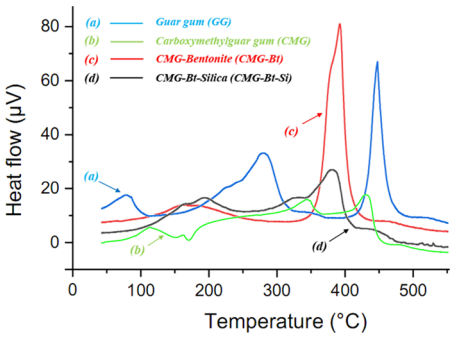

Figure 4. DTA curves of (a) GG, (b) CMG, (c) CMG-Bt, and (d) CMG-Bt-Si.

depolymerization of the chain leading to monomeric fragments; and finally, the creation of a polynuclear aromatic hydrocarbon. In Figure 3a, the curve for pure GG shows that an initial weight loss of about 24% at 121 °C is related to the moisture absorbed by the guar powder. The second main weight loss of about 45% occurs between 243 and 417 °C. This weight loss step corresponds to the decomposition of the GG structure by the degradation of the polymer backbone. The last weight loss is about 31% from 440 °C and is related to the degradation of galactomannan monomer remnants with no residue at around 537 °C.

In general, compared with the GG curve, the thermal stability of composite materials is likely to be changed due to the formation of intermolecular interactions (e.g., hydrogen bonds). The CMG thermal curve (Figure 3b) shows three main weight losses. The initial weight loss step at 119 °C, about 21%, is assigned to the moisture loss. The second step, which corresponds to the major weight loss, was about 66% at 242−453 °C. This stage refers to various decompositions, such as the cyclic degradation of saccharide units and the breaking of C−O−C glycosidic bonds in the polymeric linkages, in addition to the degradation of the carboxymethyl groups incorporated in the polymeric material. The third is a slight weight loss of about 13% from 460 °C, corresponding to the release of CO_2 from the polymer backbone and the breakage of the decomposed pyranose rings of the galactose and mannose monomers. The curve also shows that there was no residue at 520 °C.

The curves in Figure 3c,d represent, respectively, the weight losses of CMG-Bt and CMG-Bt-Si. Their thermal behavior is visible and also different from the curves of GG and GMG, starting with their initial stages of weight loss, which have around 105 and 110 °C with weight losses of about 15 and 19% related to CMG-Bt and CMG-Bt-Si, respectively. This is due to the loss of absorbed moisture and also the adsorbed moisture on the surface which seems to have required more energy. Since these aforementioned two materials have become, after cross-linking with borax along with network reinforcement with bentonite and fumed silica, materials of superabsorbent grade, this explains the complexity of this retained moisture loss.

The curve of CMG-Bt presented also a second weight loss of about 45% at 350 °C and a third large step at 350−560 °C at about 35% of weight loss, and finally, a residue of 5% is presented at 600 °C. In combination with the decomposition of the organic structures, as well as depending on the amount of bentonite in the material, it can be caused by dehydroxylation reactions of the high iron montmorillonite, aside from the dehydroxylation reactions and the decomposition of the functional groups inserted in the clay mineral support. The CMG-Bt-Si curve exhibited a long second weight with a residual of 25% at 600 °C. This weight loss was a three-step form of weight losses of about 35, 9, and 12% at 260−448, 450−464, and 500−530 °C, respectively. These weight loss steps correspond to the previous decompositions related to the bentonite added to the three-dimensional network, as well as to the fumed silica particles that are stable to heating, while the superabsorbent material lost its weight gradually; this is due to the organic nature of the guar backbone. However, the amount of residue can be attributed to the inclusion of fumed silica particles during the strengthening of the organic matrix.

As seen in Figure 4, these statements could be confirmed from the DTA curves for four materials by the appearance of exothermic peaks attributed to water loss, dehydroxylation reactions, polymer backbone rupture, and decomposition of the sugar rings remaining as monomers at the end of the combustion. Notably in the DTA thermogram, as designated in Figure 4, the exothermic characteristic peaks at 283 and 451 °C were attributed to the decomposition phase between 243−417 and 440−470 °C, respectively, in the GG thermogravimetric curve. Similarly for CMG, the exothermic peaks at 342 and 432 °C were attributed to the decomposition phase between 242 and 453 °C. However, the peaks at 395−388 °C are related to weight loss in the range of 242−453 °C and 260−448 °C, respectively, in CMG-Bt and CMG-Bt-Si thermograms.

3.2.5. X-ray Diffraction Analysis. XRD was used to analyze the crystal structure in materials. Studying the crystal structure identifies the crystal phases and provides information about the chemical modification performed. The XRD patterns of GG (a), CMG (b), CMG-Bt (c), and CMG-Bt-Si (d) are shown in Figure 5. The diffractograms in Figure 5a show a broad peak centered around 20.03° which was found to correspond to

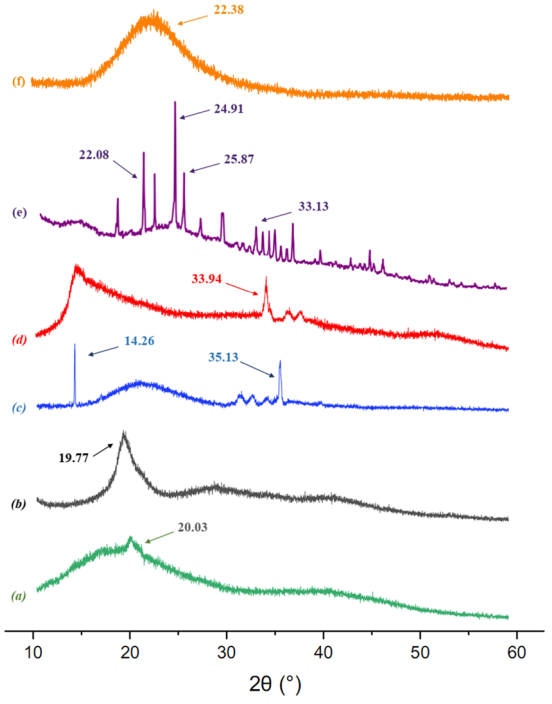

Figure 5. XRD patterns of (a) GG, (b) CMG, (c) CMG-Bt, (d) CMG-Bt-Si, (e) pure bentonite, and (f) fumed silica.

https://doi.org/10.1021/acsomega.2c04744
ACS Omega 2022, 7, 39002−39018

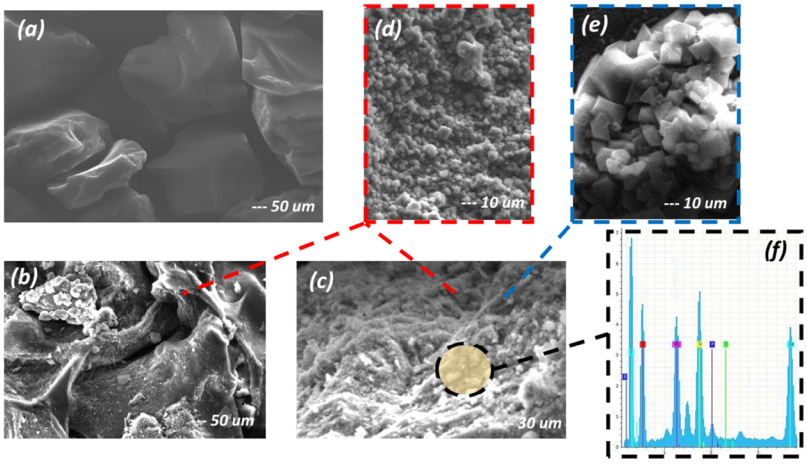

Figure 6. SEM images of (a) GG, (b) CMG-Bt, (c) CMG-Bt-Si, (d) pure bentonite, and (e) fumed silica and (f) EDX analysis of CMG-Bt-Si.

GG; indeed, it is evident that pure GG has slight crystallinity due to the crystal structure due to the interactions of −OH groups. A similar appearance has been reported for GG in the literature.[66] As can be seen in Figure 5b, CMG illustrated a broad peak at 19.77°, which explains that after the carboxymethylation reaction, a clear reduction in lattice crystallinity occurs. As it is well known, hydrogen bonds support the stability of the crystalline form of the gum, and when broken, it could lead to a reduction in crystallinity due to the fact of the change of the (−OH) groups by the carboxymethyl groups. Thus, it was clarified that the crystallinity of CMG was decreased, which supports the formation of the carboxymethyl GG material.

The CMG-Bt pattern (Figure 5c) shows a characteristic peak at 14.26° and a series of sharp peaks ranging from 30.55 to 36° with a characteristic peak at 35.13°. This shows a diminution of crystallinity; this loss of crystallinity could be attributed to the effect of replacement of hydroxyl groups by B−O bonds as a result of the borax cross-linking reaction. While the CMG-Bt solution is cross-linked with borax, the pattern shows the low intensity of the characteristic broad peak due to the consumption of the hydroxyl groups of the CMG by borate ions. As it is well known, in general, hydrogen bonds support the stability of the crystalline form of the gum, and when ruptured, this can lead to a reduction in crystallinity. As mentioned earlier, the cross-linking reaction led to the formation of a three-dimensional network that is partially crystalline; therefore, it tends to become an amorphous system. It should also be noted that the appearance of the sequence of peaks, in the scheme of Figure 5c, between a group of sharp and broad peaks in the 30.55−36° region, is related to the addition of bentonite to the cross-linked system.

Figure 5d illustrates a CMG-Bt-Si pattern that shows, in addition to the previous characteristic peaks, a broad peak between 15 and 22° and another at 33.94°. A peak around 22° for pure silica is confused with a broad peak, since pure fumed silica also has an amorphous state, which expands the nondifference between CMG-Bt and CMG-Bt-Si patterns, which subsequently ensured the anhydrous crystal structure of the superabsorbent material. As a result, the same conclusions drawn from CMG-Bt can also be applied to CMG-Bt-Si. As it is well known, pure bentonite is composed mainly of montmorillonite in addition to other minor components such as quartz and feldspar. This is supported by the XRD pattern of pure bentonite (Bt) by peaks shown in Figure 5e (22.08°, 24.91°, 25.87°, and 33.13°).[67] Finally, Figure 5f represents a fumed silica (Si) pattern that reveals a characteristic broad peak centered at 22.38°.[68]

3.2.6. Morphology Analysis. SEM analysis was performed to describe the surface morphology of the materials. SEM images of GG (a), CMG-Bt (b), CMG-Bt-Si (c), pure bentonite (d), and fumed silica (e) and EDX analysis results of CMG-Bt-Si (f) are shown in Figure 6.

In the micrograph in Figure 6a, the raw GG has an irregular, discrete, and separate granular structure such as a grain-like morphology as is widely reported. As further noticed, the modification conditions significantly affect the granular structure of the cross-linked carboxymethyl GG. The surface becomes smooth with quasi-uniform interconnected pores with increasing pore sizes; this is visible in CMG-Bt (b) and CMG-Bt-Si (c) images, with the appearance of bentonite and silica particles, which is confirmed by comparison with images (d) and (e) in Figure 6. In parallel, the topology of the reinforced cross-linked material is modified and some of the granules attach by adhering themselves. Henceforth, many small random holes can be seen on the superabsorbent material surface. In addition, some intertwined fibers in the form of a stretched pattern in addition to a porous surface can also be observed on the surface of CMG-Bt-Si images (c) due to the formation of a 3D-dimensional network.[69]

Finally, in Figure 6f, EDX analysis also confirms the formation of the superabsorbent material by the detection of new chemical elements on the surface of the material, such as boron, magnesium, silica, phosphorus, sulfur, and calcium, which come from the content of chemical elements of bentonite, borax, and fumed silica. From an overall comparison of the SEM micrographs of GG, CMG-Bt, and CMG-Bt-Si, it can be appreciated that significant modifications were made on the surface. These are called modifications that confirmed the transformation of the GG structure into CMG-Bt along with CMG-Bt-Si by the cross-linking reaction.

3.3. Analysis of the Swelling Properties of the Superabsorbent Polymer. The absorption performance of superabsorbent materials depends on several factors. These include factors that can be processed during the synthesis of the superabsorbent material, whereas other factors are related to the absorption medium. In this section, the effect of cross-linking, clay mineral, and silica particles on water absorption, as

https://doi.org/10.1021/acsomega.2c04744
ACS Omega 2022, 7, 39002−39018

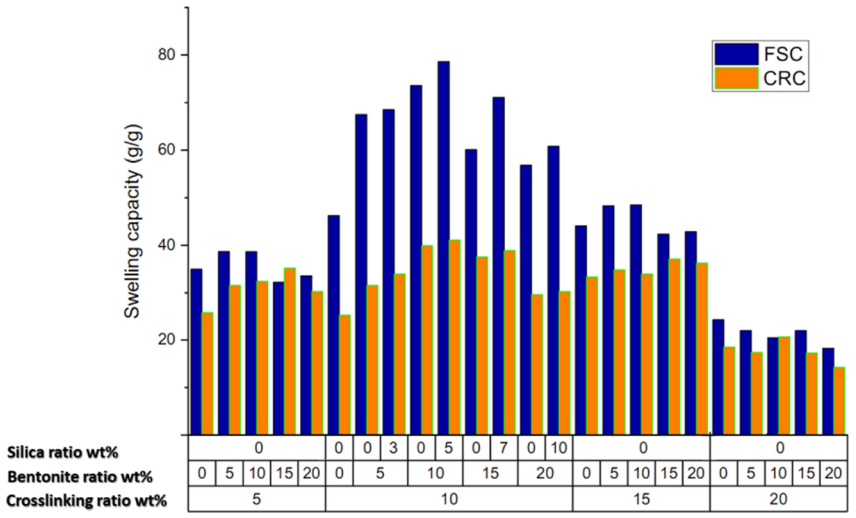

Figure 7. Swelling performances of CMG-Bt and CMG-Bt-Si versus cross-linking ratio (wt %), bentonite ratio (wt %), and silica particle ratio (wt %).

well as the effects of pH, nature of liquids, and mineral charge on water absorption were discussed.

3.3.1. Effect of Cross-Linking, Mineral Clay, and Silica Particles on Water Absorbency. 3.3.1.1. Effect of Cross-Linking. Since the ratio of cross-linkers has an impact on the water absorption of SAPs, the cross-linking reaction was performed at different weight ratios between borax and CMG. The effect of the amount of cross-linker (borax) on the water uptake capacity in the synthesis of CMG-Bt and CMG-Bt-Si was studied in deionized water to achieve the maximum performance of the synthesized material. The results shown in Table 1 and Figure 7 refer to the variation in the performance of superabsorbent materials, in terms of swelling capacity, as a function of the cross-linking ratio, the weight ratio of bentonite, and the weight ratio of silica nanoparticles.

Based on the results in Figure 7, the highest values are 78.63 g/g for FSC and 41.09 g/g for CRC, attributed to the 10 wt % cross-linking ratios. However, from a general point of view of the results, it appeared that the values of FSC and CRC increased significantly to a maximum from a cross-linking rate of 5 wt % up to 10 wt %, followed by a decrease in the values from a cross-linking rate of 15 wt % and again a further decrease to the lowest values of FSC and CRC at a cross-linking rate of 20 wt %. The explanation for this phenomenon is that the optimum degree of cross-linking was achieved at a ratio of 10 wt %, which leads to greater relaxation of the polymer chains. This leads to faster diffusion of water into the polymer matrix. However, at weight ratios higher than 10%, the FSC and CRC values of CMG-Bt are reduced when the weight ratio of the cross-linker is 15%. Therefore, at 20 wt %, the water uptake of CMG-Bt was reduced to less than even the initial cross-linker ratio (5 wt %), due to the rigidity of the synthesized structure, which prevents the extension of the polymer chains. However, this can be explained by the fact that increasing the cross-linking rate can increase the probability of generating O−B−O bonds to create more links between the CMG backbones. Consequently, the cross-linking density is promoted. As previously mentioned, cross-linking occurs between vicinal diols stereochemically on the same side (cis) of the mannose units on the CMG backbone.

In summary, the reason for this reduction in uptake may be due to the higher amount of cross-linker, which in turn promotes the generation of more cross-linking points between the polymer chains (bridging points) and then the increase in cross-linking density. As a result, the remaining space in the network to retain water molecules was minimized, as the pore size of available voids between the network chains was reduced. As a result, the slow diffusion of water molecules into the network leads to a decrease in absorption performance. As a result, a ratio of borax to CMG of about 10 wt % is deduced to be the optimized cross-linking density.

3.3.1.2. Effect of Mineral Clay. From another point of view on the results, it appears that the weight ratio of the clay mineral (bentonite) also influences the swelling capacities of the superabsorbent materials. Considering all cross-linking weight ratios, the FSC and CRC values increase with the weight ratio of bentonite from 0 to 10 wt %, followed by a decrease from 10 to 20 wt %. The increase in FSC and CRC values (from 0 to 10 wt %) can be explained by the swelling property of bentonite, which enhances the absorption capacity of superabsorbent materials. On the other hand, the antagonistic decrease with the increase of the bentonite weight ratio can be explained by the fact that starting from a certain value, the content of cationic metals in bentonite, as shown previously, favors the creation of the shielding effect inside the hydrogel, and consequently, a decrease in the absorption capacity was observed. It is assumed from the results that the maximum ratio of 10 wt % bentonite is considered to be the optimum ratio.

3.3.1.3. Effect of Incorporation of Silica Particles. Based on the above results, cross-linking weight ratio samples of the optimum value (10 wt %) were selected to investigate the effect of incorporating silica nanoparticles on the FSC and CRC performance. In Figure 7, at a cross-linking rate of 10 wt %, when comparing CMG-Bt-Si and CMG-Bt samples, in an overall perspective, the FSC and CRC values of CMG-Bt-Si (where it includes a proportion of silica nanoparticles) are increased compared to the values of CMG-Bt. This supports that the incorporation of silica nanoparticles promotes the swelling capacity performance of superabsorbent materials.

In another aspect, the swelling performance increased from 68.52 and 33.97 g/g at 3 wt % silica nanoparticles to maximum values of 78.63 and 41.09 g/g at 5 wt % silica nanoparticles for FSC and CRC, respectively. Then, a slight decrease was

https://doi.org/10.1021/acsomega.2c04744
ACS Omega 2022, 7, 39002−39018

observed from 71.09 and 38.89 g/g at 15 wt % silica nanoparticles, followed by a second decrease to 60.8 and 30.29 g/g at 20 wt % silica nanoparticles for FSC and CRC, respectively. This augmentation can be explained by the effect of the dispersion of Si═O bonds between the CMG backbone which, with the help of hydrogen bonds, favors the attraction of water (H_2O) molecules inside the matrix of the hydrogel. However, from a weight ratio of 5% of silica particles, it is noticed that the absorption performance started to decrease. Hence, this reduction may be due to the increase of the silanol bonds inside the material matrix that encourages new physical bonds between the Si═O bonds coming from the silica nanoparticles and the hydroxyl -OH bonds of the CMG skeleton, which, in other words, creates a cross-linking continuity inside the hydrogel matrix, thus affecting a decrease in absorption performance according to the same explanations discussed above.

3.3.2. Effect of pH on Water Absorbency. Generally, the ionic strength of the affected solution has a significant influence on the water absorption of SAPs. Therefore, the effect of pH on the water uptake of CMG-Bt-Si under optimal conditions has been investigated, and the results are presented in Figure 8. Based on the findings of the study of the effect of

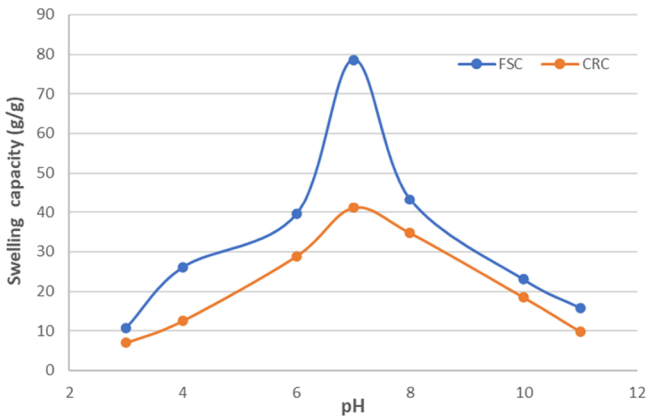

Figure 8. Effect of pH on the water uptake of CMG-Bt-Si.

cross-linking, mineral clay, and silica particles on water uptake, the CMG-Bt-Si sample with the highest FSC and CRC values was chosen to investigate the water absorption variation as a function of pH.

Following the FSC and CRC methods described above, the study was performed with a slight modification of the immersion time. The equilibrium swelling rate was studied for 2.5 h at different pHs (3.0−11.0), allowing the synthesized products to reach the maximum absorption. The desired pH steps at 3.0, 4.0, 6.0, 7.0, 8.0, 10.0, and 11.0 were obtained by diluting hydrochloric acid (pH 1.0) and sodium hydroxide (pH 13.0) solutions with distilled water. The buffer solutions are not suitable for pH adjustment because the ions present in the buffer solution affect the ionic strength of SAPs. The swelling behavior shown by the obtained results indicates that in the range of 3.0 to 7.0, the pH was increased from 10.83 and 7.0 g/g to 71.68 and 41.09 g/g by FSC and CRC, respectively, reaching the maximum uptake at pH 6.8. However, similarly, the values were greatly reduced to 15.81 and 12.5 g/g at pH 11.0. As it is known, the immersion of water in the SAP matrix is achieved by the fact that water molecules diffuse into the SAP network through the interaction of water molecules with the functional ionic groups. In addition, due to the electrostatic repulsion effect between the charges of the polymer chains, the dimensions of the sample are increased, which explains the observed swelling. In the pH range of 6.5 to 7.5, the carboxylic acid groups are slightly ionized, and subsequently, the repulsive forces between the carboxylate anions increase. On the other hand, the hydrogen bonds between the carboxylic acid groups were at the optimal density and the water uptake increased.

By varying the pH values to 11, the water uptake becomes negligibly lower. This phenomenon can be explained by three different hypotheses. First, in an acidic environment, during absorption, a reversible borax cross-linking reaction can take place. Therefore, the deterioration of oxygen−borax−oxygen cross-links, and then, the risk of loss of the cross-linked network will be highly probable. Second, the protonation of the carboxylate anions to the carboxylic acid form applies a decrease in the repulsive forces between the carboxylate anions as well as an increase in the stiffness of the polymer matrix due to the resulting increase in hydrogen bonding density. Third, the decrease in water uptake under basic conditions can also be explained by the fact that the carboxylate anions were formed by ionization of the carboxyl groups, and then, the electrostatic repulsion in the network decreases due to the screening effect of sodium ions. Therefore, as the pH increases, this phenomenon leads to the collapse of the polymer matrix.

3.3.3. Effect of Liquid Nature on Superabsorbent Material Performance. Based on the same previous approach, CMG-Bt, and CMG-Bt-Si samples, with the optimum cross-linking weight ratio (10 wt %), were chosen to study the effect of liquid nature on water absorption. The swelling study was conducted using the previously reported methods. The absorption and retention capacity results of CMG-Bt and CMG-Bt-Si in distilled water, tap water, and saline solution are shown in Figure S2.

First of all, it is evident from the results that all the FSC and CRC values of the CMG-Bt-Si samples, which contain the silica nanoparticles, are higher than those of the CMG-Bt samples by keeping the cross-linking weight ratio of bentonite in saline, tap water, and distilled water constant, and this is adequate with the previous conclusions, which confirms them as well, referring to the example of the sample CMG-Bt-Si 02 which showed the best swelling performance (cross-linking ratio 10 wt %, weight ratio of bentonite 10 wt %, and silica nanoparticles 5 wt %). The sample exhibited absorption values (FSC) of 78.63, 60.85, and 42.15 g/g as well as retention values (CRC) of 41.09, 39.49, and 27.5 g/g in saline solution, tap water, and distilled water, respectively. This leads to two important observations; the first one is that the absorption, represented by the FSC results, is always higher than the retention which is presented by the CRC performances. The second observation is that the performance of absorption and retention decreases when switching from tests in distilled water, or tap water, to saline solution. However, these two variations are applied to all samples. The absorption capacity values are lower than the retention capacity values, which is explained by the fact that unbound free water droplets attached to the outer surface of swollen samples have increased mobility compared to bound and semibound water in the sample matrix, which, as a result, can be easily lost during centrifugation.

The SAP has several application areas that are exposed to different types of water, namely, saline solution, tap water, and distilled water. As shown in Figure 2S, the absorbance

https://doi.org/10.1021/acsomega.2c04744
ACS Omega 2022, 7, 39002−39018

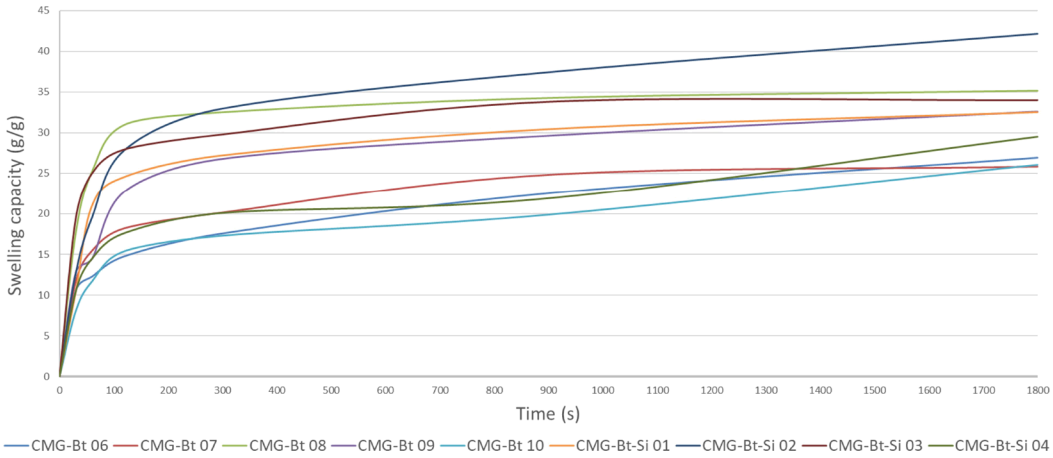

Figure 9. Absorption kinetics of CMG-Bt & CMG-Bt-Si samples: Absorption rate (AR) in 0.9 wt % NaCl solution.

decreases as the ion content of the solution tester increases. A higher concentration of sodium ions in the saline solution would disturb the hypotonic equilibrium by causing a strong shielding effect of additional Na^+ ions, which decreases the osmotic pressure difference between the SAP matrix and the external solution, with a consequent decrease in absorbance results. In addition, the abundant sodium ion in high concentration saline solution, not to mention tap water and distilled water, can penetrate the swollen SAP, reducing the efficiency of the carboxylate carbonyl ion, decreasing the hydrophilicity, and repelling the hydrophilic groups. Thus, the absorption should be measured under different conditions to evaluate the swelling properties.

3.3.4. Swelling Kinetics and Equilibrium Water Absorption of Superabsorbent Materials. Figure 9 presents the absorption of CMG-Bt and CMG-Bt-Si samples in a saline solution as a function of time. The AR of superabsorbent samples initially rises rapidly for 1200 s and then begins to stabilize by reaching a near plateau, so that the swelling equilibrium capacity has been reached. For SAP samples, high values of absorption capacities are required. CMG-Bt-Si 02 and CMG-Bt-Si 03 show excellent performance, respectively. The weakest performance is attributed to CMG-Bt 10 which slowly increases. The other samples have relatively the same curve format.

However, the absorption kinetics can be expressed by the "Voigt-based viscoelastic model" as shown in eq 7:[70]

$$A_t = A_\infty (1 - \exp(-t/\zeta) \quad (7)$$

where A_t (g/g) is the uptake at time t, A_∞ (g/g) is the power parameter (g/g), indicating the theoretical water uptake at equilibrium, t (s) is the uptake time, and ζ (s) represents the velocity parameter, representing the time required to reach 63% of the water uptake at equilibrium. The values of A_∞ and ζ were calculated by fitting the experimental data by eq 7, as shown in Table 2. Namely, ζ is a measure of the resistance to water permeation; lower values of ζ reflect a higher AR.

As shown in Table 2, the highest value of ζ (261 s) was attributed to CMG-Bt 06 as opposed to CMG-Bt-Si 02 and CMG-Bt-Si 03, which have the lowest values of ζ (41 and 45 s, respectively). The sample with no content of bentonite and silica (CMG-Bt 06) showed a slower absorption. Then, the AR increases with the incorporation of bentonite which appeared in the samples CMG-Bt 07−09 with an exception of the sample CMG-Bt 10 which shows an AR value around 192 s,

Table 2. Absorption Kinetics of Superabsorbents CMG-Bt (6−10) and CMG-Bt-Si (1−4)

superabsorbent material	sample	A_∞ (g/g)	ζ (s)
CMG-Bt	CMG-Bt 06	26.97	261
	CMG-Bt 07	25.81	73
	CMG-Bt 08	32.15	90
	CMG-Bt 09	32.6	93
	CMG-Bt 10	26.05	192
CMG-Bt-Si	CMG-Bt-Si 01	32.54	58
	CMG-Bt-Si 02	42.15	41
	CMG-Bt-Si 03	34.01	45
	CMG-Bt-Si 04	29.5	61

which is possibly due to the excess of bentonite content which can increase the osmotic pressure and consequently disfavors the absorption of the salt solution. However, CMG-Bt-Si samples showed relatively improved AR performance.[71] Indeed, an increase in the AR would be expected from the increase in contact area with the decrease in SAP particle size and mineral content. It is known that the AR of SAP is strongly influenced by the SAP particle size principally; with smaller particle size, a higher AR is observed.[6]

3.3.5. Effect of Mineral Charge on Urea Absorption. The FTIR spectra of urea (a), CMG-Bt (b), and CMG-Bt-Si (c) are shown in Figure 10. The spectrum of urea (a) shows the characteristic bands of pure urea. The N−H symmetric stretching vibrations appear as a broadband in the wavenumber

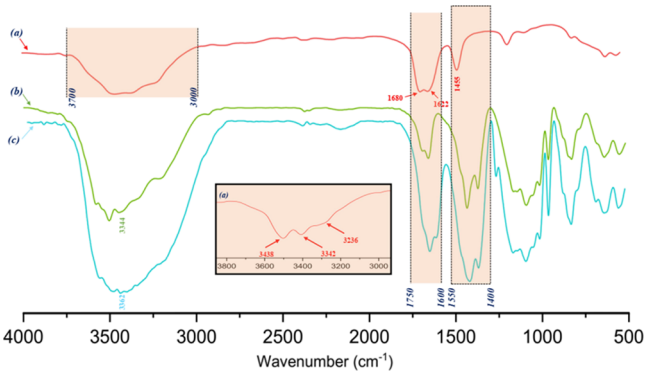

Figure 10. FTIR spectra of (a) urea, (b) CMG-Bt-urea, and (c) CMG-Bt-Si-urea.

https://doi.org/10.1021/acsomega.2c04744
ACS Omega 2022, 7, 39002−39018

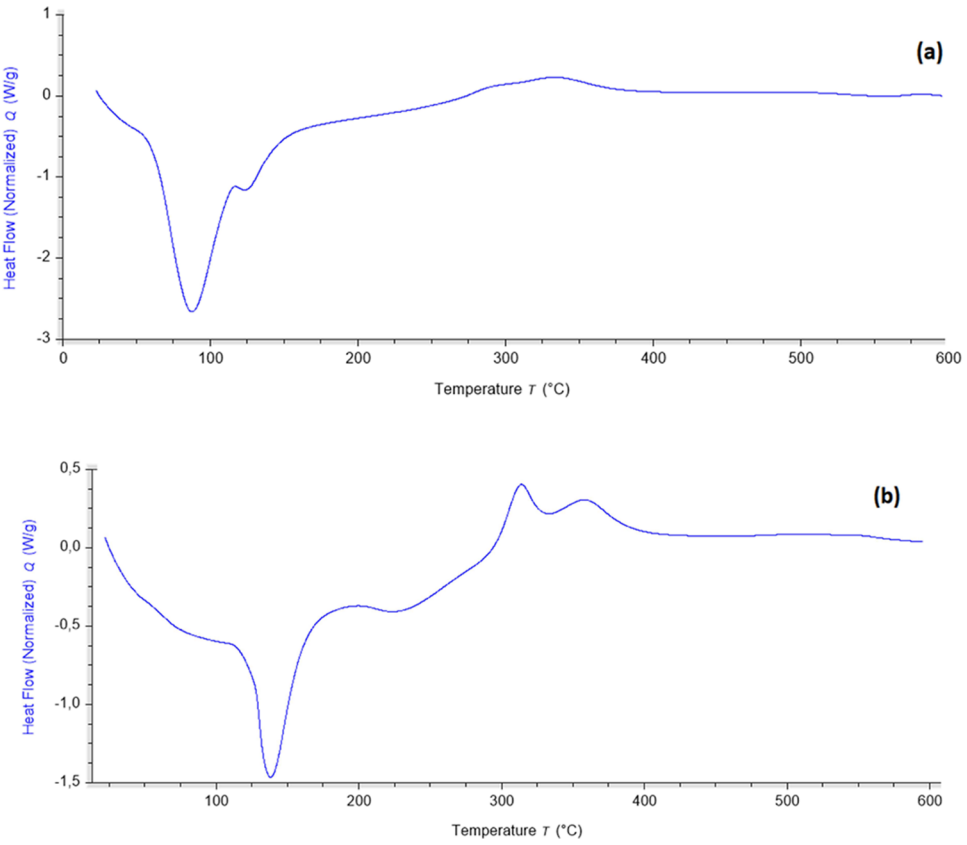

Figure 11. DSC thermograms of (a) pure CMG-Bt-Si and (b) urea-absorbing CMG-Bt-Si sample.

range between 3600 and 3000 cm^{-1} centered around 3438 and 3342 cm^{-1}, while the N−H bond deformation frequencies appear at 1622 cm^{-1}. The characteristic stretching vibrations of the C═O appear at 1680 cm^{-1}. In addition, a characteristic band that appears at 1453 cm^{-1} was related to the C−N bond stretching. FTIR spectra (b) and (c) are related to the superabsorbent materials CMG-Bt and CMG-Bt-Si after absorption of the urea test, focusing on the intervals 1750−1600 and 1550−1400 cm^{-1} of the three spectra in Figure 10. It can be concluded that the appearance of the characteristic urea bands (C═O and C−N), which did not exist before absorption in the hydrogel matrix, in addition to a remarkable high intensity on the spectrum of (c) CMG-Bt-Si compared to CMG-Bt. This proves the influence of silica on the absorption of urea through the hydrogen bonding between the Si−OH hydroxyl group on one side and also the C═O and N−H carboxyl groups of urea on the other. These observations signify the presence of urea inside the superabsorbent material after the urea absorption test.

DSC analysis was also used as a technique to confirm the absorption of urea molecules. DSC thermograms of pure CMG-Bt-Si (a) and urea-absorbing samples (b) are shown in Figure 11. In both samples, changes and differences are observed between 20 and 600 °C. In addition, the endotherm around 100 °C is shown in both DSC thermographs, which is related to the evaporation of moisture and absorbed impurities. The DSC thermograph of the CMG-Bt-Si urea-absorbing sample (b) shows two exothermic transitions between 300 and 380 °C, at 0.405 and 0.306 W/g, respectively, which are not shown in the DSC thermographs of pure CMG-Bt-Si (a). So, the drop between these two exothermic curves may indicate a decomposition that may be related to the thermal and oxidative decomposition of urea molecular parts as well as the strong intermolecular hydrogen bonding between the attractive groups of the material backbone.

Table 3 presents the results of elemental analysis of CMG-Bt-Si in the pure state and another sample of CMG-Bt-Si after absorption of the urea test. The results demonstrate the appearance of 7.34% nitrogen in the CMG-Bt-Si sample after urea absorption in contrast to the pure CMG-Bt-Si sample with a percentage of 0.16%, and the remaining percentage can be attributed to the traces of nitrogen derived from the bentonite content. However, the increase in nitrogen content is due to traces of decomposition of the urea incorporated in the superabsorbent material. Henceforth, the add-on nitrogen content found in the CMG-Bt-Si sample may confirm the affinity of the material to absorb urea molecules and supports the inference discussed above. Briefly, the FTIR results allow us to conclude that the silica particles incorporated inside the material relatively promote the absorption of urea. Furthermore, both the DSC and elemental analysis results significantly reinforce this conclusion.

Table 3. Elemental Analysis GG and CMG

polymer sample	% of carbon	% of nitrogen
CMG-Bt-Si (neat)	39.1	0.16
CMG-Bt-Si (absorbing urea)	37.71	7.34

4. CONCLUSIONS

The objective of this study was to synthesize a new highly absorbent material based on carboxymethyl GG which would further be reinforced with bentonite as a clay filler and silica

https://doi.org/10.1021/acsomega.2c04744
ACS Omega 2022, 7, 39002−39018

particles to increase the absorption capacity of the material to make it competitive and even propose it as an alternative to the conventional absorbents used in commercial disposable hygiene products. Two different types of materials have been successfully prepared: CMG-Bt and CMG-Bt-Si (Figure S3). As regards the structural characterization of the synthesized materials, the ^{1}H NMR and ^{13}C NMR analyses have confirmed the successful formation of CMG by the carboxymethylation process. The ^{1}H NMR analysis has also been carried out to investigate the partial DS which was 0.19. The FTIR analysis confirmed the formation of the synthesized superabsorbent materials. TGA and DTA thermograms illustrated a difference in the thermal stabilities of GG, CMG, CMG-Bt, and CMG-Bt-Si. The XRD analysis confirmed the synthesis of the materials by showing the difference in crystallinity between GG, CMG, CMG-Bt, and CMG-Bt-Si due to the cross-linking along with the inclusion of bentonite containing crystalline parts of montmorillonite and the effect of the incorporation of silica particles. SEM micrographs showing significant visible modifications have been obtained for the surface of GG, CMG-Bt, and CMG-Bt-Si. EDX analyses allowed the detection of new chemical elements on the surface of the material.

The synthesis parameters (cross-linking ratio, mineral clay ratio, and incorporation of silica particles) revealed a significant effect on water absorption. The maximum swelling properties were 78.63 and 41.09 g/g for FSC and CRC, respectively. These results were attributed to the optimal parameters of 10 wt % cross-linking rate, 10 wt % of bentonite, and 5 wt % of silica nanoparticles. Indeed, the incorporation of silica nanoparticles promoted the swelling capacity performance of superabsorbent materials by comparing the results of CMG-Bt-Si with CMG-Bt. The effect of pH on water uptake has been studied. The CMG-Bt-Si samples have reached the maximum absorption at pH 6.8 with progressively lower values tending to extreme acids and bases. CMG-Bt-Si in the contents of 5 and 7% in silica particles show velocity parameters (ζ) of 41 and 45 s, respectively, which has given them better swelling kinetics. The FTIR and DSC analyses confirm not only the existence but also the retention of urea within the three-dimensional network of the superabsorbent material. Besides, the elemental analysis of the CMG-Bt-Si sample after the urea uptake test showed an increase of 7.18% in nitrogen content. This support confirmed the affinity of CMG-Bt-Si to absorb urea molecules.

To sum up, this study also presents certain limits, such that from a rate cross-linking of 15 wt %, the performance becomes mediocre instead of the rest of the parameters. Also, from 15 wt % silica, the polymer becomes less rigid, undergoes mechanical influences, and loses the form of a hydrogel. In order to achieve appropriate results and better promote the use of synthesized products, some additional investigations are recommended such as absorption tests in different types of liquids (artificial blood, bovine blood, etc.). In other respects, more effective tests on the properties of hydrogels are also advisable, such as the absorption under load, compressive test, gel fraction, and rheological test.

■ ASSOCIATED CONTENT

Supporting Information

The Supporting Information is available free of charge at https://pubs.acs.org/doi/10.1021/acsomega.2c04744.

^{1}H NMR spectra of pure GG (a), CMG (b), and ^{13}C NMR spectra of pure GG (c), and CMG (d); swelling behavior in different media; ^{1}H NMR shift related to the determination of the DS; and photographs of the superabsorbent materials (PDF)

■ AUTHOR INFORMATION

Corresponding Author

Yahya Bachra − *Laboratory of Analytical and Molecular Chemistry (LCAM), Faculty of Sciences Ben M'Sick, Department of Chemistry and Innovations and Technologies Platform (PInTech), University Hassan II of Casablanca, Casablanca 20000, Morocco;* orcid.org/0000-0003-0449-256X; Email: yahya.bachra10@gmail.com, yahya.bachra@umontreal.ca

Authors

Ayoub Grouli − *Laboratory of Analytical and Molecular Chemistry (LCAM), Faculty of Sciences Ben M'Sick, Department of Chemistry and Innovations and Technologies Platform (PInTech), University Hassan II of Casablanca, Casablanca 20000, Morocco*

Fouad Damiri − *Laboratory of Analytical and Molecular Chemistry (LCAM), Faculty of Sciences Ben M'Sick, Department of Chemistry, University Hassan II of Casablanca, Casablanca 20000, Morocco*

X. X. Zhu − *Department of Chemistry, University of Montreal, Montreal H3C 3J7 QC, Canada;* orcid.org/0000-0003-0828-299X

Mohammed Talbi − *Laboratory of Analytical and Molecular Chemistry (LCAM), Faculty of Sciences Ben M'Sick, Department of Chemistry and Innovations and Technologies Platform (PInTech), University Hassan II of Casablanca, Casablanca 20000, Morocco*

Mohammed Berrada − *Laboratory of Analytical and Molecular Chemistry (LCAM), Faculty of Sciences Ben M'Sick, Department of Chemistry and Innovations and Technologies Platform (PInTech), University Hassan II of Casablanca, Casablanca 20000, Morocco*

Complete contact information is available at: https://pubs.acs.org/10.1021/acsomega.2c04744

Notes

The authors declare no competing financial interest.

■ ACKNOWLEDGMENTS

The authors are very grateful to the Platform for Innovations and Technologies (PInTech) and the Center for Doctoral Studies (CEDoc) of the Faculty of Sciences Ben M'Sick (Morocco) for their support of the present work. The authors acknowledge the support from the Canada Research Chairs program and the CREATE program from NSERC of Canada in the form of a scholarship to Y.B. from the PrEEmiuM project. Finally, the authors would like to thank the staff of the Departments of Chemistry and Biological Sciences of the University of Montreal (in particular G. Beaudoin; A. Sanseigne; F. Langlois; P. Li; X. Fan; Q. Wang; C. Malveau; N. Macia; and D. Bélanger) for their assistance in achieving the research's findings.

■ ABBREVIATIONS

AR: absorption rate; CMG: carboxymethyl guar gum; CMG-Bt: carboxymethyl guar-bentonite; CMG-Bt-Si: carboxymethyl guar-bentonite-silica; CRC: centrifuge retention capacity; DS:

https://doi.org/10.1021/acsomega.2c04744
ACS Omega 2022, 7, 39002−39018

degree of substitution; DSC: differential scanning calorimetry; EDX: energy-dispersive X-ray spectroscopy; FSC: free swell capacity; FTIR: Fourier transform infrared spectroscopy; GG: guar gum; NMR: nuclear magnetic resonance; SAP: superabsorbent polymer; SEM: scanning electron microscope; TDA: thermodifferential analysis; TGA: thermogravimetric analysis; ζ: velocity parameter; wt %: percentage by weight; XRD: X-ray diffraction

REFERENCES

(1) Zohuriaan-mehr, M. J.; Kabiri, K. Superabsorbent Polymer Materials: A Review. *Iran. Polym. J.* **2008**, *17*, 451−477. http://journal.ippi.ac.ir

(2) Fouad, D.; Bachra, Y.; Ayoub, G.; Ouaket, A.; Bennamara, A.; Knouzi, N.; Berrada, M.A Novel Drug Delivery System Based on Nanoparticles of Magnetite Fe3O4 Embedded in an Auto Cross-Linked Chitosan. In *Chitin and Chitosan - Physicochemical Properties and Industrial Applications*; IntechOpen, 2020; pp 1−14.

(3) Mignon, A.; de Belie, N.; Dubruel, P.; van Vlierberghe, S. Superabsorbent Polymers: A Review on the Characteristics and Applications of Synthetic, Polysaccharide-Based, Semi-Synthetic and 'Smart' Derivatives. *Eur. Polym. J.* **2019**, *117*, 165−178.

(4) Damiri, F.; Kommineni, N.; Ebhodaghe, S. O.; Bulusu, R.; Jyothi, V. G. S. S.; Sayed, A. A.; Awaji, A. A.; Germoush, M. O.; Al-Malky, H. S.; Nasrullah, M. Z.; Rahman, M. H.; Abdel-Daim, M. M.; Berrada, M. Microneedle-Based Natural Polysaccharide for Drug Delivery Systems (DDS): Progress and Challenges. *Pharmaceuticals* **2022**, *15*, 190.

(5) Damiri, F.; Rahman, M. H.; Zehravi, M.; Awaji, A. A.; Nasrullah, M. Z.; Gad, H. A.; Bani-Fwaz, M. Z.; Varma, R. S.; Germoush, M. O.; Al-Malky, H. S.; Sayed, A. A.; Rojekar, S.; Abdel-Daim, M. M.; Berrada, M. MXene (Ti3C2Tx)-Embedded Nanocomposite Hydrogels for Biomedical Applications: A Review. *Materials* **2022**, *15*, 1666.

(6) Bachra, Y.; Grouli, A.; Damiri, F.; Bennamara, A.; Berrada, M. A New Approach for Assessing the Absorption of Disposable Baby Diapers and Superabsorbent Polymers: A Comparative Study. *Results Mater.* **2020**, *8*, 14.

(7) Damiri, F.; Bachra, Y.; Bounacir, C.; Laaraibi, A.; Berrada, M. Synthesis and Characterization of Lyophilized Chitosan-Based Hydrogels Cross-Linked with Benzaldehyde for Controlled Drug Release. *J. Chem.* **2020**, *2020*, 1−10.

(8) Ruel-Gariépy, E.; Shive, M.; Bichara, A.; Berrada, M.; le Garrec, D.; Chenite, A.; Leroux, J. C. A Thermosensitive Chitosan-Based Hydrogel for the Local Delivery of Paclitaxel. *Eur. J. Pharm. Biopharm.* **2004**, *57*, 53−63.

(9) Venkatachalam, D.; Vediappan, V.; Kaliappa Gounder, S. Synthesis and Evaluation of Trimethylolpropane Triacrylate Cross-linked Superabsorbent Polymers for Conserving Water and Fertilizers. *J. Appl. Polym. Sci.* **2013**, *129*, 1350−1361.

(10) Vuong, L. D.; Quang, D. A.; Chuc, N. H.; van Luan, L.; Bao, V. V. Q.Natural Gums as a Sustainable Source for Synthesizing Copper Nanoparticles. In *Copper Nanostructures: Next-Generation of Agrochemicals for Sustainable Agroecosystems*; 2022; pp 81−98.

(11) Padil, V. V. T.; Wacławek, S.; Černík, M.; Varma, R. S. Tree Gum-Based Renewable Materials: Sustainable Applications in Nanotechnology, Biomedical and Environmental Fields. *Biotechnol. Adv.* **2018**, *36*, 1984−2016.

(12) Taib, M.; Damiri, F.; Bachra, Y.; Berrada, M.; Bouyazza, L.Recent Advances in Micro-and Nanoencapsulation of Bioactive Compounds and Their Food Applications. In *Nanotechnology in Intelligent Food Packaging*; Bhattacharya, T., Shakeel, A., Eds.; Scrivener Publishing LLC, 2022; pp 271−290.

(13) Bangar, S. P.; Kaushik, N.Functional Cereals: Functional Components and Benefits. In *Functional Cereals and Cereal Foods*; Springer International Publishing: Cham, 2022; pp 3−25.

(14) Maier, H.; Anderson, M.; Karl, C.; Magnuson, K.; Whistler, R. L., Guar Locust Bean, Tara, And Fenugreek Gums. In *Industrial Gums: Polysaccharides and Their Derivatives: Third Edition*; BeMiller, J., Whistler, R., Eds.; Academic Press, 1993; pp 181−226.

(15) Tamo, A.; Bachra, Y.; Grouli, A.; Damiri, F.; Benhar, S.; Bennamara, A.; Berrada, M.; Talbi, M. A Novel Quantitative Method For The Validation Of The Dosage Of Amnesic Shellfish Poisoning Toxins In Bivalve Mollusks. *Nat. Volatiles Essent. Oils* **2021**, *8*, 2858−2869.

(16) Verbeken, D.; Dierckx, S.; Dewettinck, K. Exudate Gums: Occurrence, Production, and Applications. *Appl. Microbiol. Biotechnol.* **2003**, *63*, 10−21.

(17) Gupta, A. P.; Verma, D. K. Synthesis and Characterization of Carboxymethyl Guar Gum Nanoparticles Stabilized Polyaniline/Carboxymethyl Guar Gum Nanocomposites. *J. Nanostruct. Chem.* **2015**, *5*, 405−412.

(18) Thombare, N.; Mishra, S.; Shinde, R.; Siddiqui, M. Z.; Jha, U. Guar Gum Based Hydrogel as Controlled Micronutrient Delivery System: Mechanism and Kinetics of Boron Release for Agricultural Applications. *Biopolymers* **2021**, *112*, No. e23418.

(19) Mudgil, D.; Barak, S.; Khatkar, B. S. Guar Gum: Processing, Properties and Food Applications - A Review. *J. Food Sci. Technol.* **2014**, *51*, 409−418.

(20) Zhang, S.; Peng, Y.; Jiang, R.; Liu, W.; Yang, H.; Yun, N.; Chai, X. Predicting the Swelling Behavior of Acrylic Superabsorbent Polymers Used in Diapers. *Adv. Polym. Technol.* **2021**, *2021*, No. 9999826.

(21) Zuraida, S.; Dewancker, B. J.; Margono, R. B. Calculation Formula in Determining Recycling of Disposable Diapers Waste as Concrete Composite Materials. *IOP Conf. Ser. Earth Environ. Sci.* **2021**, *847*, No. 012014.

(22) Płotka-Wasylka, J.; Makoś-Chełstowska, P.; Kurowska-Susdorf, A.; Treviño, M. J. S.; Guzmán, S. Z.; Mostafa, H.; Cordella, M. End-of-Life Management of Single-Use Baby Diapers: Analysis of Technical, Health and Environment Aspects. *Sci. Total Environ.* **2022**, *836*, No. 155339.

(23) Liu, T. G.; Wang, Y. T.; Li, B.; Deng, H. B.; Huang, Z. L.; Qian, L. W.; Wang, X. Urea Free Synthesis of Chitin-Based Acrylate Superabsorbent Polymers under Homogeneous Conditions: Effects of the Degree of Deacetylation and the Molecular Weight. *Carbohydr. Polym.* **2017**, *174*, 464−473.

(24) Yu, Y.; Liu, L.; Kong, Y.; Erchi, Z.; Liu, Y. Synthesis and Properties of N -Maleyl Chitosan-Cross-Linked Poly (Acrylic Acid-Co-Acrylamide) Superabsorbents. *J. Polym. Environ.* **2011**, *19*, 926−934.

(25) Lacoste, C.; Lopez-Cuesta, J. M.; Bergeret, A. Development of a Biobased Superabsorbent Polymer from Recycled Cellulose for Diapers Applications. *Eur. Polym. J.* **2019**, *116*, 38−44.

(26) Arredondo, R.; Yuan, Z.; Sosa, D.; Johnson, A.; Beims, R. F.; Li, H.; Wei, Q.; Xu, C. C.Performance of a Novel, Eco-Friendly, Cellulose-Based Superabsorbent Polymer (Cellulo-SAP): Absorbency, Stability, Reusability, and Biodegradability. *Can. J. Chem. Eng.***2022**, DOI: 10.1002/CJCE.24601.

(27) Xiao, X.; Yu, L.; Xie, F.; Bao, X.; Liu, H.; Ji, Z.; Chen, L. One-Step Method to Prepare Starch-Based Superabsorbent Polymer for Slow Release of Fertilizer. *Chem. Eng. J.* **2017**, *309*, 607−616.

(28) Hasija, V.; Sharma, K.; Kumar, V.; Sharma, S.; Sharma, V. Green Synthesis of Agar/Gum Arabic Based Superabsorbent as an Alternative for Irrigation in Agriculture. *Vacuum* **2018**, *157*, 458−464.

(29) Kulanthaivel, S.; Rathnam, S. V.; Agarwal, T.; Pradhan, S.; Pal, K.; Giri, S.; Maiti, T. K.; Banerjee, I. Gum Tragacanth-Alginate Beads as Proangiogenic-Osteogenic Cell Encapsulation Systems for Bone Tissue Engineering. *J. Mater. Chem. B* **2017**, *5*, 4177−4189.

(30) Bachra, Y.; Grouli, A.; Damiri, F.; Talbi, M.; Berrada, M. A Novel Superabsorbent Polymer from Crosslinked Carboxymethyl Tragacanth Gum with Glutaraldehyde: Synthesis, Characterization, and Swelling Properties. *Int. J. Biomater.* **2021**, *2021*, 1−14.

(31) Behrouzi, M.; Moghadam, P. N. Synthesis of a New Superabsorbent Copolymer Based on Acrylic Acid Grafted onto Carboxymethyl Tragacanth. *Carbohydr. Polym.* **2018**, *202*, 227−235.

(32) Khushbu; Warkar, S. G.; Kumar, A. Synthesis and Assessment of Carboxymethyl Tamarind Kernel Gum Based Novel Super-

https://doi.org/10.1021/acsomega.2c04744
ACS Omega 2022, 7, 39002−39018

absorbent Hydrogels for Agricultural Applications. *Polymer* **2019**, *182*, No. 121823.
(33) Yang, H.; Wu, L.; Liu, J.; Wang, W. The Re-Swelling Mechanism of Superabsorbent Polymers (SAP) in the SAP Voids of Cement-Based Materials. *Cem. Concr. Compos.* **2022**, *130*, No. 104561.
(34) Zhang, W.; Wang, P.; Deng, Y.; He, X.; Yang, X.; Chen, R.; Lei, Z. Preparation of Superabsorbent Polymer Gel Based on PVPP and Its Application in Water-Holding in Sandy Soil. *J. Environ. Chem. Eng.* **2021**, *9*, No. 106760.
(35) Mazlan, S. N. A.; Abd Rahim, S.; Ghazali, S.; Jamari, S. S. Optimization of N,N'-Methylenebis(Acrylamide), and Ammonium Persulfate Content in Carbonaceous/Acrylic Acid-Co-Acrylamide Superabsorbent Polymer. *Mater. Today Proc.* **2021**, *57*, 1088.
(36) Hibino, T. Facile Synthesis of Layered Double Hydroxide/Superabsorbent Polymer Composites for Water and Wastewater Treatment. *Appl. Clay Sci.* **2021**, *211*, No. 106188.
(37) Zhang, W.; Guo, L.; Liu, Q.; Yang, M.; Chen, J.; Lei, Z. Preparation and Properties of a Biodegradability Superabsorbent Composite Based on Flax Cake Protein-g-Poly (Acrylic Acid)/Kaolinite. *J. Appl. Polym. Sci.* **2022**, *139*, 51975.
(38) Kwon, Y. R.; Kim, H. C.; Kim, J. S.; Chang, Y. W.; Park, H.; Kim, D. H. Itaconic-Acid-Based Superabsorbent Polymer with High Gel Strength and Biocompatibility. *Polym. Int.* **2022**, *71*, 1090.
(39) Hasan, A. M. A.; Keshawy, M.; Abdel-Raouf, M. E. S. Atomic Force Microscopy Investigation of Smart Superabsorbent Hydrogels Based on Carboxymethyl Guar Gum: Surface Topography and Swelling Properties. *Mater. Chem. Phys.* **2022**, *278*, No. 125521.
(40) Mir, T. A.; Ali, A.; Mazumdar, N. Glycerol-Crosslinked Guar Gum Monoaldehyde Based Superabsorbent Hydrogels for Vitamin B6 (Pyridoxine Hydrochloride) Delivery. *Polym. Bull.* **2022**, *2022*, 1−28.
(41) Li, S.; Chen, G. Agricultural Waste-Derived Superabsorbent Hydrogels: Preparation, Performance, and Socioeconomic Impacts. *J. Cleaner Prod.* **2020**, *251*, No. 119669.
(42) Dagar, V.; Pahwa, R.; Ahuja, M. Preparation and Characterization of Calcium Cross-Linked Carboxymethyl Tamarind Kernel Polysaccharide as Release Retardant Polymer in Matrix. *Biointerface Res. Appl. Chem.* **2023**, *13*, 111.
(43) Dodi, G.; Hritcu, D.; Popa, M. I. Carboxymethylation of Guar Gum: Synthesis and Characterization. *Cellul. Chem. Technol.* **2011**, *45*, 171−176.
(44) Pan, X.; Wang, Q.; Ning, D.; Dai, L.; Liu, K.; Ni, Y.; Chen, L.; Huang, L. Ultraflexible Self-Healing Guar Gum-Glycerol Hydrogel with Injectable, Antifreeze, and Strain-Sensitive Properties. *ACS Biomater. Sci. Eng.* **2018**, *4*, 3397.
(45) Thombare, N.; Jha, U.; Mishra, S.; Siddiqui, M. Z. Borax Cross-Linked Guar Gum Hydrogels as Potential Adsorbents for Water Purification. *Carbohydr. Polym.* **2017**, *168*, 274−281.
(46) Liu, C.; Lei, F.; Li, P.; Jiang, J.; Wang, K. Borax Crosslinked Fenugreek Galactomannan Hydrogel as Potential Water-Retaining Agent in Agriculture. *Carbohydr. Polym.* **2020**, *236*, No. 116100.
(47) Ait Hmeid, H.; Akodad, M.; Aalaoul, M.; Baghour, M.; Moumen, A.; Skalli, A.; Anjjar, A.; Conti, P.; Sfalanga, A.; Ryazi Khyabani, F.; Minucci, S.; Daoudi. Clay Mineralogy, Chemical and Geotechnical Characterization of Bentonite from Beni Bou Ifrour Massif (the Eastern Rif, Morocco). *Geol. Soc., London, Spec. Publ.* **2020**, *502*, SP502-2019-2025.
(48) Zhang, J.; Yuan, K.; Wang, Y. P.; Gu, S. J.; Zhang, S.; Tang. Preparation and Properties of Polyacrylate/Bentonite Superabsorbent Hybrid via Intercalated Polymerization. *Mater. Lett.* **2007**, *61*, 316−320.
(49) Li, Z.; Barnes, J. C.; Bosoy, A.; Stoddart, J. F.; Zink, J. I. Mesoporous Silica Nanoparticles in Biomedical Applications. *Chem. Soc. Rev.* **2012**, *41*, 2590−2605.
(50) Forny, L.; Saleh, K.; Denoyel, R.; Pezron, I. Contact Angle Assessment of Hydrophobic Silica Nanoparticles Related to the Mechanisms of Dry Water Formation. *Langmuir* **2010**, *26*, 2333−2338.
(51) Videira-Quintela, D.; Guillen, F.; Martin, O.; Cumbal, L.; Montalvo, G. Antibacterial and Antioxidant Triple-Side Filler Composed of Fumed Silica, Iron, and Tea Polyphenols for Active Food Packaging. *Food Control* **2022**, *138*, No. 109036.
(52) Xie, W. Q.; Yu, K. X.; Gong, Y. X. A Fast and Simple Headspace Gas Chromatographic Technique for Quantitatively Analyzing Urea in Human Urine. *Anal. Biochem.* **2019**, *576*, 9−12.
(53) Berardesca, E.; Cameli, N. Non-Invasive Assessment of Urea Efficacy: A Review. *Int. J. Clin. Pract.* **2020**, *74*, 13603.
(54) Andersen, F. A. Final Report of the Safety Assessment of Urea. *Int. J. Toxicol.* **2005**, *24*, 1−56.
(55) Lavertu, M.; Xia, Z.; Serreqi, A. N.; Berrada, M.; Rodrigues, A.; Wang, D.; Buschmann, M. D.; Gupta, A. A Validated 1H NMR Method for the Determination of the Degree of Deacetylation of Chitosan. *J. Pharm. Biomed. Anal.* **2003**, *32*, 1149−1158.
(56) Berrada, M.; Chevigny, S.; Thibodeau, C.Polysaccharide Phyllosilicate Absorbent or Superabsorbent Nanocomposite Materials. US 20050214541A1, 2005.
(57) Dodi, G.; Pala, A.; Barbu, E.; Peptanariu, D.; Hritcu, D.; Popa, M. I.; Tamba, B. I. Carboxymethyl Guar Gum Nanoparticles for Drug Delivery Applications: Preparation and Preliminary in-Vitro Investigations. *Mater. Sci. Eng., C* **2016**, *63*, 628−636.
(58) Badwaik, H. R.; Kumari, L.; Maiti, S.; Sakure, K.; Ajazuddin; Nakhate, K. T.; Tiwari, V.; Giri, T. K. A Review on Challenges and Issues with Carboxymethylation of Natural Gums: The Widely Used Excipients for Conventional and Novel Dosage Forms. *Int. J. Biol. Macromol.* **2022**, *209*, 2197−2212.
(59) Gao, J.; Grady, B. P. Reaction Kinetics and Subsequent Rheology of Carboxymethyl Guar Gum Produced from Guar Splits. *Ind. Eng. Chem. Res.* **2018**, *57*, 7345.
(60) Heinze, T.; Pfeiffer, K.; Lazik, W. Starch Derivatives with High Degree of Functionalization. III. Influence of Reaction Conditions and Starting Materials on Molecular Structure of Carboxymethyl Starch. *J. Appl. Polym. Sci.* **2001**, *81*, 2036−2044.
(61) Yu, Y.; Jia, F.; Li, S.; Yan, S.; Leng, C.; Yuan, K. Synthesis and Swelling Behavior of Superabsorbents Cross-Linked with N-Maleyl Chitosan. *Int. J. Polym. Mater. Polym. Biomater.* **2013**, *62*, 450−454.
(62) Chen, J.; Wu, J.; Raffa, P.; Picchioni, F.; Koning, C. E. Superabsorbent Polymers: From Long-Established, Microplastics Generating Systems, to Sustainable, Biodegradable and Future Proof Alternatives. *Prog. Polym. Sci.* **2022**, *125*, No. 101475.
(63) Ma, M.; Mukerabigwi, J. F.; Huang, R.; Lei, S.; Huang, X.; Cao, Y. Eco-Friendly Superabsorbent Synthesis Based on Polysaccharides. *J. Polym. Environ.* **2020**, *28*, 2801−2809.
(64) Gupta, A. P.; Verma, D. K. Preparation and Characterization of Carboxymethyl Guar Gum Nanoparticles. *Int. J. Biol. Macromol.* **2014**, *68*, 247−250.
(65) Elsaeed, S. M.; Zaki, E. G.; Omar, W. A. E.; Ashraf Soliman, A.; Attia, A. M. Guar Gum-Based Hydrogels as Potent Green Polymers for Enhanced Oil Recovery in High-Salinity Reservoirs. *ACS Omega* **2021**, *6*, 23421.
(66) Mudgil, D.; Barak, S.; Khatkar, B. S. X-Ray Diffraction, IR Spectroscopy and Thermal Characterization of Partially Hydrolyzed Guar Gum. *Int. J. Biol. Macromol.* **2012**, *50*, 1035−1039.
(67) Zhirong, L.; Azhar Uddin, M.; Zhanxue, S. FT-IR and XRD Analysis of Natural Na-Bentonite and Cu(II)-Loaded Na-Bentonite. *Spectrochim. Acta, Part A* **2011**, *79*, 1013−1016.
(68) Chen, X.; Huang, Q.; Hao, W.; Ding, C.; Wang, Y.; Zeng, H. Controlling of Fumed Silica Particle Size Uniform Production Process Based on Burner Fluid Dynamic Simulation. *Ind. Eng. Chem. Res.* **2022**, *61*, 7235.
(69) Damiri, F.; Bachra, Y.; Berrada, M. Synthesis and Characterization of 4-Formylphenylboronic Acid Cross-Linked Chitosan Hydrogel with Dual Action: Glucose-Sensitivity and Controlled Insulin Release. *Chin. J. Anal. Chem.* **2022**, *50*, No. 100092.
(70) Wang, W.; Zhang, J.; Wang, A. Preparation and Swelling Properties of Superabsorbent Nanocomposites Based on Natural Guar Gum and Organo-Vermiculite. *Appl. Clay Sci.* **2009**, *46*, 21−26.

https://doi.org/10.1021/acsomega.2c04744
ACS Omega 2022, 7, 39002−39018

(71) Pourjavadi, A.; Kurdtabar, M. Collagen-Based Highly Porous Hydrogel without Any Porogen: Synthesis and Characteristics. *Eur. Polym. J.* **2007**, *43*, 877−889.

https://doi.org/10.1021/acsomega.2c04744
ACS Omega 2022, 7, 39002−39018